Phosphoproteomic Analysis Identifies REPS1 as an Insulin- and Exercise-Responsive Signal Transducer to Glucose Uptake in Skeletal Muscle

Jeppe Kjærgaard[1], Cecilie B. Lindqvist[1], Júlia Prats Quesada[1], Søren Jessen[2], Farina Schlabs[1], Amy M. Ehrlich[1], Caio Y. Yonamine[1], Mario García-Ureña[1], Johann H. Schmalbruch[1], Lewin Small[1], Martin Thomassen[2], Anders Krogh Lemminger[2], Kasper Eibye[2], Alba Gonzalez-Franquesa[1], Jacob V. Stidsen[3], Kurt Højlund[3,4], Juleen R. Zierath[1,5,6], Tuomas O. Kilpeläinen[1], Jens Bangsbo[2], Jonas T. Treebak[1], Morten Hostrup[2,#], Atul S. Deshmukh[1,#].

[1] Novo Nordisk Foundation Center for Basic Metabolic Research, Faculty of Health and Medical Sciences, University of Copenhagen, Copenhagen, Denmark

[2] The August Krogh Section for Human Physiology, Department of Nutrition, Exercise and Sports, University of Copenhagen, Copenhagen, Denmark

[3] Steno Diabetes Center Odense, Odense University Hospital, Odense C, Denmark

[4] Department of Clinical Research, University of Southern Denmark, Odense C, Denmark

[5]Department of Physiology and Pharmacology, Integrative Physiology, Karolinska Institutet, Stockholm, Sweden

[6]Department of Molecular Medicine and Surgery, Integrative Physiology, Karolinska Institutet, Stockholm, Sweden

Short running title: REPS1 in insulin & exercise signaling in skeletal muscle

Key words: Skeletal muscle signaling, phosphoproteomics, glucose metabolism

Figures: 6

Word count: 4782

References: 77

#Corresponding authors:

Atul S Deshmukh

Novo Nordisk Foundation Center for Basic Metabolic Research, Faculty of Health and Medical Sciences, University of Copenhagen, Blegdamsvej 3B, DK2200, Copenhagen, Denmark

Phone: +45 35 32 53 13; e-mail: atul.deshmukh@sund.ku.dk

Morten Hostrup

The August Krogh Section for Human Physiology, Department of Nutrition, Exercise and Sports, University of Copenhagen, Universitetsparken 13, DK2100, Denmark

Phone: +45 24 47 47 85; e-mail: mhostrup@nexs.ku.dk

Abstract

Skeletal muscle glucose uptake is regulated in response to insulin and exercise, critical factors for metabolic health. We conducted a comprehensive phosphoproteomic analysis of skeletal muscle from healthy individuals in response to an acute bout of exercise or insulin stimulation during a hyperinsulinemic euglycemic clamp. Our analysis identified 233 phosphosites regulated by both stimuli, most of which showed opposite regulation. However, 71 phosphosites on 55 proteins exhibited similar regulation, suggesting a convergence of exercise and insulin signaling pathways. Notably, the vesicle-associated protein, REPS1, was highly phosphorylated at Ser709 in response to both insulin and exercise, and this phosphorylation was closely linked to insulin-stimulated glucose uptake. Insulin-induced REPS1 Ser709 phosphorylation, mediated by p90 ribosomal S6 kinase (RSK), was impaired in insulin resistant mice and humans. Collectively, REPS1 is a convergence point for insulin and exercise signaling, presenting a potential therapeutic target for treating insulin resistance.

Introduction

Skeletal muscle is the largest tissue in the human body and plays a pivotal role in maintaining glucose homeostasis and energy metabolism. One of its primary metabolic functions is glucose uptake and utilization, which is essential for normal physiological processes and is particularly relevant in the context of metabolic disorders, such as type 2 diabetes (T2D)[1]. Impaired insulin-stimulated skeletal muscle glucose uptake is a hallmark of insulin resistance and is a central feature of the pathogenesis of T2D[2]. Skeletal muscle glucose uptake is intricately regulated by multiple signaling pathways that dictate its delivery, transport, and metabolism[3–5]. Glucose transporter 4 (GLUT4) plays a central role in glucose uptake[6,7]. During unstimulated conditions GLUT4 predominantly resides within intracellular vesicles. However, in response to insulin or exercise, GLUT4-containing vesicles translocate to the plasma membrane[5]. This suggests that exercise- and insulin-induced GLUT4 translocation rely on commonly regulated distal mechanisms and protein machinery. However, the specific signal transducers through which insulin and exercise mediate glucose uptake represent a critical knowledge gap.

Studies on human skeletal muscle in people with T2D have revealed an impairment in insulin signaling pathways targeting GLUT4, while exercise-mediated signals remain largely intact[8–10]. The study of insulin signaling has mainly been limited to two major pathways: phosphatidylinositol 3-kinase (PI3K)-AKT and RAC1-p21-activated kinase (PAK) pathways, which are recognized as vital modulators of glucose transport[11–13]. In contrast, exercise-mediated glucose uptake is mainly orchestrated through signaling mechanisms integrating a spectrum of mechanical, chemical, and stress signals[14–18]. One hypothesis is that insulin and exercise-triggered signaling converge at distal nodes to meet common cellular needs, including glucose import. This notion was supported by the discovery of the molecular switches, TBC1D1 and TBC1D4, which intricately regulate the action of insulin and exercise on the intercellular trafficking of GLUT4 and lipid transporter-containing vesicles to the cell surface[19–22]. Intriguingly, an acute bout of exercise can potentiate subsequent insulin signaling, notably by the AMPK-TBC1D4 axis in both human and rodent skeletal muscle[23–25]. Despite these few examples, the understanding of these converging distal mechanisms and the shared protein machinery remains incomplete and underexplored.

Recent improvements in mass spectrometry (MS)-based phosphoproteomics have advanced the study of dynamic protein signaling[26–28]. Pioneering studies in skeletal muscle have unveiled extensive signaling networks activated by both exercise and insulin[29–31]. Despite these valuable insights, the intricate interplay among these pathways and connection to GLUT4 remains to be fully elucidated. A comprehensive understanding of these interactions is crucial for unraveling

therapeutic targets that can increase skeletal muscle glucose uptake in diseases characterized by insulin resistance. Based on the current evidence, we hypothesized that a core set of proteins, modulated by phosphorylation in response to both insulin and exercise, form a fundamental regulatory nexus for skeletal muscle glucose uptake.

We conducted a phosphoproteomic analysis in skeletal muscle from healthy individuals in response to an acute bout of exercise or insulin stimulation by a hyperinsulinemic euglycemic clamp. While the majority of phosphosites regulated by both insulin and exercise displayed opposite responses to the stimulus, we identified 71 sites on 55 proteins that were regulated in the same direction, potentially influencing glucose uptake. Notably, we found RalBP1-associated Eps domain-containing protein 1 (REPS1), a vesicle-associated protein, was phosphorylated in response to both insulin and exercise. We provide evidence that REPS1 is crucial for glucose uptake in skeletal muscle, with its phosphorylation dependent on P90S6 kinase (RSK). Moreover, insulin action on REPS1 S709 phosphorylation was impaired in several *in vivo* models of insulin resistance and strongly correlated with insulin sensitivity. Our results position REPS1 at the intersection of insulin and exercise signaling, advancing the understanding of the molecular mechanisms regulating skeletal muscle glucose uptake.

Results

Phosphoproteomic Signature of Insulin and Exercise Signaling in Human Skeletal Muscle

To accurately capture signaling events in response to insulin and exercise, we conducted two experimental trials, in randomized order, separated by 1-2 weeks on eight healthy males (age, 18–36 yrs., lean mass index, 14–22 kg/m2; maximal oxygen uptake [VO2max], 40–60 ml/kg/min). Given our objective to identify converging distal signaling events in response to insulin and exercise, we conducted both trials on the same individuals to minimize potential inter-subject variations in insulin and exercise signaling. During the experimental trials, participants underwent either a 2-h hyperinsulinemic euglycemic clamp (HEC) or performed a single bout of high-intensity cycling exercise for 10 min at maximal effort (Figure 1A). We collected vastus lateralis muscle biopsies immediately before and after HEC or exercise on the experimental days. The acute bout of exercise reduced glycogen stores ($P < 0.01$), while no change was observed with insulin stimulation (Figure 1B). The levels of plasma epinephrine and norepinephrine rose during exercise but were unchanged during the clamp procedure (Figure S1A-D). Conversely, plasma insulin levels were only increased during the clamp but unchanged during the acute bout of exercise (Figure S1E-F). Insulin stimulation increased leg glucose uptake ($P < 0.001$, Figure 1C).

We confirmed the activation of canonical insulin and exercise-induced signaling pathways in the muscle biopsies by Western blot analysis (Figure 1D). For instance, both insulin and acute exercise induced phosphorylation of mTOR at S2448, while insulin specifically increased p-AKT at S473 and exercise specifically increased p-AMPK at T172 and p-ACC at S221 (Figure 1D & Figure S1G-J).

Subsequently, we performed in-depth analysis of the phosphoproteome in insulin and exercise-stimulated skeletal muscle. Proteomic analysis of skeletal muscle is inherently challenging due to the presence of highly abundant contractile proteins hindering the detection of lowly abundant proteins [32]. To overcome this, we employed stable isotope labelling with 11-plex Tandem Mass Tag (TMT), phosphopeptide enrichment, and phosphopeptide-level fractionation prior to tandem mass spectrometry (LC-MS/MS). This approach allowed a comprehensive phosphoproteome in human skeletal muscle and the quantification of 13,717 phosphopeptides (11,934 phosphosites localization probability > 0.75) on 3,368 proteins (Figure 1E). Principal component analysis demonstrated clustering of samples by subject on component 1 and by stimulus on component 2 (Figure 1F-G). Differential abundance analysis of the phosphoproteome revealed significant regulation with 805 and 4,784 sites changing in response to insulin and exercise, respectively (False-discovery rate (FDR) < 0.05, Figure 1H-I). This included known insulin- (upregulation of RPS6 S236/T241, TBC1D4 S341, TSC2 S939 and downregulation of GYS1 S645) and exercise-signaling proteins (upregulation of STIM1 S257, ACACB S222 and downregulation of PDHA1 S300) as well as new insulin signaling proteins, such as the S741 phosphosite on the RNA-binding protein 15, RBM15, which was downregulated in response to insulin. Interestingly, RBM15 was recently associated with liver insulin resistance through epigenetic m6A regulation[33]. Our comprehensive phosphoproteomic analysis encompassing insulin and exercise stimuli in the same individuals represents a valuable resource for the scientific community (Supplementary table 1A-C).

Shared and Distinct Features of Insulin and Exercise Signaling

To decipher the signaling pathways and regulatory networks activated by insulin and exercise, we investigated if specific kinases were activated and potentially responsible for the observed phosphorylation events in our dataset. Recent work on mapping substrates of the human Ser/Thr kinome has provided *in vitro* evidence of kinase-substrate relationship[34]. Leveraging this work, we overlaid our sequence windows surrounding phosphorylated serine and threonine residues with the *in vitro*-predicted kinase motifs. As substrates are essential for interaction with their upstream kinase, we filtered for kinases known to be expressed in skeletal muscle tissue[35].

Subsequently, we performed a kinase enrichment analysis, predicting activation of known kinases (P70S6K, P90S6K/RSK, SGK1), and a hitherto new insulin-activated kinase, PIM3, in response to insulin (Figure 2A, Supplementary table 1E). Exercise resulted in activation of known kinases such as PKACA, AMPKα1, AMPKα2, MAPKAPK2, MAPKAPK3, RSK2 (Figure 2B, Supplementary table 1F) and new exercise kinases such as QIK (also known as salt-inducible kinase 2, SIK-2). Phosphosites regulated by exercise were enriched for processes related to protein degradation, protein conformation and protein activation/inhibition while those regulated by insulin were associated with intracellular localization (two-sided fishers exact test $P < 0.05$) (Figure 2C). Furthermore, sites with a reported function in molecular associations (i.e., interactions) or disease-associated function were enriched by both insulin and exercise (Figure 2C).

To elucidate the crosstalk between insulin and exercise-induced signaling, we filtered for significantly altered sites by both insulin and exercise (< 5% FDR in both comparisons). In total, this analysis revealed 233 phosphosites that were regulated either in the same or opposite direction (Figure 2D & Supplementary table 1C-D). When examining individual responses to exercise and insulin, we observed that the majority of phosphosites, 162 in total, were regulated in opposite directions, compared to 71 sites regulated in the same direction. This highlights the major role of insulin and exercise in regulating muscle anabolic and catabolic metabolism, respectively. One example is the known T246 site of AKT1S1 (also known as PRAS40), which was phosphorylated in response to insulin stimulation and dephosphorylated on the same site in response to exercise (Figure 2E). Conversely, SH3BP4, a protein involved in autophagy and receptor endocytosis, displayed dephosphorylation on S246 in response to insulin and phosphorylation in response to exercise[36]. Exercise and insulin are known to induce and attenuate autophagy in skeletal muscle, respectively[37,38]. Therefore, the S246 phosphorylation on SH3BP4 could be a key regulatory step in skeletal muscle autophagy.

We hypothesized that the phosphosites regulated in the same direction during insulin and exercise, could be involved in metabolic processes such as skeletal muscle glucose uptake. Accordingly, these sites were enriched for biological processes related to exocytosis, actin filament organization and endomembrane system organization (Figure S2A). Similarly, sites downregulated with both stimuli were enriched for cytoskeletal organization (Figure S2B). Exploring specific examples, we observed that SORBS1 (also known as Cbl-associated protein/CAP) was dephosphorylated on both S949/S953 (same phosphopeptide) in response to both insulin and exercise (Figure 2E). SORBS1 is required for insulin-stimulated glucose uptake

in adipocytes independent of the canonical PI3K pathway[39]. However, its role in skeletal muscle insulin signaling has been debated. Additionally, we observed that CLIP-associating protein (CLASP)-2 S370 phosphorylation was induced in response to both insulin and exercise (Figure 2E), while CLASP2 S327 was dephosphorylated in response to both stimuli (Figure S2C). When we visualized the AlphaFold predicted structure, we found both sites to be present in the same loop domain suggesting interdependency (Figure 2F). The same observation was seen on the sister-protein CLASP1 at S600 and S559 (Figure S2D-E). CLASP2 is required for insulin-stimulated GLUT4 translocation, thereby serving as a positive readout for our phoshoproteomics analysis[40,41]. In total, we identified 29 phosphosites across 27 proteins induced by both insulin and exercise. To gain further insights into their upstream kinases, we conducted a motif enrichment analysis, revealing a prevalent sequence motif surrounding the phosphosites with a highly significant proportion of arginine at position -3 (Odds Ratio = 4, P = 5e-05) (Figure 2G). Additionally, these motifs were enriched for P70S6K and P90S6K (RSKs) kinases (Figure 2H). Interestingly, prior research has shown that S6K and RSK are activated by both insulin and exercise in human skeletal muscle[42–45]. In addition, RSK1 was recently found to induce GLUT4 translocation in adipocytes through TBC1D4 phosphorylation in response to stress stimuli[46]. Of particular interest, we identified the protein RalBP1-associated Eps domain-containing protein 1 (REPS1), to be phosphorylated on S709 in response to insulin and exercise (Figure 2I).

The Insulin and Exercise-responsive Protein, REPS1, is a Critical Regulator of Skeletal Muscle Glucose Uptake

In our search for novel signal transducers of glucose uptake, we identified REPS1 S709 was phosphorylated in response to both insulin and exercise stimuli. The amino acid sequence surrounding serine 709 was found to be conserved from zebrafish to human containing the motif favored by AGC kinases[47,48] (Figure 3A). Moreover, REPS1 has been characterized for its involvement in endocytosis[47]. Therefore, we prioritized REPS1 for further studies to validate novel signal transducers mediating glucose uptake in skeletal muscle. We validated our observation by immunoblotting for phospho-REPS1 at S709 in human skeletal muscle, confirming an increase in phosphorylated REPS1 at S709 in response to both insulin and exercise (Figure 3B-C). Strikingly, REPS1 S709 phosphorylation (Post-Pre clamp) correlated tightly with steady-state leg glucose uptake with a squared Pearson's correlation coefficient of 0.86 (P < 0.001) (Figure 3D). In contrast, p-AKT S473 and p-mTOR S2448, classical markers of insulin signaling, showed poor correlation (Figure S3A-B). To assess the association of REPS1 S709 phosphorylation with glucose uptake during exercise in human skeletal muscle *in vivo*, we examined REPS1 S709

phosphorylation in muscle biopsies obtained prior to and after a one-legged exercise and compared this with corresponding femoral arterial-venous plasma glucose balance. REPS1 S709 phosphorylation displayed a small but significant modest ($P < 0.05$) increase immediately after 10 minutes of exercise (Figure S3C & S3E). However, the REPS1 phosphorylation was not associated with glucose uptake in the exercised leg ($r^2 = 0.01$, $P = 0.85$) (Figure S3D). This suggests a close association between insulin-stimulated skeletal muscle glucose uptake and REPS1 709 phosphorylation, wherewith exercise potentially influencing this response.

To ascertain the conservation of response, we anaesthetized C57BL/6NTac male mice and surgically stimulated one leg to contract while the contralateral leg remained rested. Upon contractions, mice were injected with either saline or 15 mU insulin combined with ^{3}H-2-deoxyglucose for 15 minutes. Tibialis Anterior (TA) muscle had a ~20-fold and 3.4-fold increase in glucose uptake during contractions and insulin, respectively, however, no additive effect was observed (Figure 3E). We also measured REPS1 S709 phosphorylation and found increased phosphorylation in all contracted muscles in response to 15 minutes of *in situ* contraction (main effect $P < 0.001$) (Figure 3F & H). As observed in humans, 15 minutes of *in vivo* insulin stimulation increased REPS1 S709 phosphorylation (main effect $P < 0.05$). The insulin-stimulated glucose uptake into TA muscle had a strong correlation with REPS1 S709 phosphorylation ($r^2 = 0.63$, $P = 0.0063$) (Figure 3G) whereas contraction-stimulated glucose uptake showed poor correlation ($r^2 = -0.064$, $P = 0.58$) (Figure S3F). To test if REPS1 is required for insulin-stimulated glucose uptake, we transfected C2C12 muscle cells with small interfering RNA (siRNA) against mouse *Reps1*. Efficient knockdown of *Reps1* was validated at the protein level by Western blot analysis ($p<0.01$), without any changes in GLUT4 expression (Figure 3I). Insulin-stimulated ^{3}H-2-deoxyglucose was impaired when REPS1 protein expression was reduced (Interaction $P < 0.01$) (Figure 3J). Collectively, these findings provide evidence to suggest that REPS1 is a point of convergence for insulin and exercise signaling in skeletal muscle.

RSK is an Upstream Kinase of REPS1 S709 and is Associated with Vesicle-Sorting Proteins in Skeletal Muscle

We hypothesized that a single upstream kinase could be activated during insulin and exercise stimulation and be responsible for the increased phosphorylation of REPS1 S709. Interestingly, the sequence motifs of phosphosites upregulated by both insulin and exercise were enriched for the P70S6K and P90S6K isoforms (Figure 2H). In support, a recent study found that RSK can phosphorylate REPS1 at S709 *in vitro* in 293T cells[49]. To investigate if RSK is involved in insulin-stimulated glucose uptake, we preincubated C2C12 myotubes with the RSK inhibitor, BI-D1870,

for 20 minutes followed by 10 minutes of maximal insulin stimulation. Glucose uptake, REPS1 S709 phosphorylation was increased in response to insulin, however, these insulin-induced effects were blunted in cells where RSK was inhibited (interaction $P = 0.003$, $P = 0.075$) (Figure 4A-C). Importantly, the RSK inhibitor lowered phosphorylated REPS1 without affecting insulin-stimulated phosphorylation of AKT on S473 (Figure S4A). Furthermore, the basal level of phosphorylated REPS1 on S709 was lowered suggesting RSK is the upstream kinase. Using L6-GLUT4-myc model, we next investigated whether REPS1 phosphorylation is required for translocation of GLUT4 to cell surface. We confirmed that the reduced insulin-stimulated glucose uptake by blocking RSK-REPS1 signaling was due to an impaired GLUT4 translocation to the plasma membrane (interaction $P = 0.018$, Figure 4D).

To translate these findings into adult intact muscle, we dissected soleus muscle from mice and incubated with or without the addition of a submaximal insulin dose (300μIU/ml) in the presence or absence of RSK inhibitor (10 μM, 1 hour pre-incubation). Notably, RSK inhibitor impaired insulin-stimulated glucose uptake and REPS1 phosphorylation (interaction $P = 0.04$, Figure 4E). We also confirmed REPS1 phosphorylation was impaired in same muscles (interaction $P = 0.068$, Figure 4F), despite full activation of the AKT pathway (Figure 4G-H).

To test whether insulin-induced REPS1 S709 phosphorylation is also dependent on the mTOR-S6K pathway, we stimulated C2C12 myotubes with Rapamycin and PF-4708671, known inhibitors of mTORC1 or P70S6K, respectively. These inhibitors reduced insulin-stimulated phosphorylation of P70S6K T389 (mTOR site) and RPS6 S235/236 (P70S6K site), without affecting REPS1 S709 phosphorylation (Figure S4B-D). As RSK can also be activated by 3-phosphoinositide-dependent protein kinase 1 (PDK1), we pre-treated cells with a PDK1 inhibitor, MK-7, but found no impairment in insulin-stimulated phosphorylation of REPS1 S709 despite markedly reduced phosphorylation of the PDK1 site, T308 on AKT (Figure S4E-G). RSK is also known to be activated through the RAF-MEK-ERK pathway[50,51] (Figure 4J, left). Therefore, we inhibited the MAPK-pathway and observed concurrent reduction in ERK1/2 T202/Y204 (interaction $P < 0.001$) and REPS1 S709 phosphorylation (interaction $P = 0.02$) indicating that signaling from the insulin receptor to REPS1 S709 is mediated through the MAPK pathway (Figure S4H-J).

The S709 residue of REPS1 lies within a disordered region where phosphorylation could trigger gain/loss of protein-interactions. To identify REPS1 binding partners, we applied adeno-associated virus (AAV) assisted overexpression of FLAG-control or FLAG-*Reps1*. We next performed mass spectrometry-based interaction proteomics. As expected, REPS1 was the most

enriched protein in the WT-Flag IP vs CTR-Flag (Figure 4I). RALBP1, a protein recently shown to bind REPS1 and regulate GLUT4-exocytosis in fibroblast, co-precipitated with REPS1 in our screen[52]. Furthermore, all five subunits of the endocytotic adaptor protein 2 (AP-2) complex (Ap2a1, Ap2a2, Ap2b1, Ap2m1 and Ap2s1) and associated kinases, Aak1, Bmp2k, were bound to REPS1. These interactors were similarly found by immunoprecipitation and MS-based proteomics of endogenous REPS1 (Figure S4K). The REPS1 interactors confidently found in both Flag and endogenous immunoprecipitation were enriched for processes related to endocytosis and vesicle transport (Figure S4L-M). In summary, we show that REPS1 binds to proteins related to both the exocytosis and endocytosis machinery (Figure 4J, right), and RSK acts as an upstream kinase for REPS1.

Insulin-induced REPS1 S709 Phosphorylation *in vivo* is Impaired in Multiple Models of Insulin Resistance

After establishing the critical role of REPS1 in skeletal muscle glucose uptake, we sought to investigate whether REPS1 phosphorylation is impaired under insulin resistant conditions. To elucidate if insulin-stimulated phosphorylation of REPS1 is affected by insulin resistance, we fed C57BL/6NTac male mice a low-fat diet (LFD) or high-fat diet (HFD) for 16 weeks, injected them acutely with saline or insulin (1U/kg) and tested their blood glucose levels before and 15 minutes following injection (Figure 5A). Mice fed a HFD had higher body weight ($P < 0.001$) and, upon insulin injection, displayed less reduction in blood glucose compared to LFD-fed mice (interaction $P < 0.05$, Figure 5B), indicating reduced whole-body insulin sensitivity in the HFD group. Intriguingly, the insulin-stimulated phosphorylation of REPS1 at S709 was lower in mice fed a HFD compared to those fed a LFD (interaction $P < 0.05$) (Figure 5C). This effect was specific to skeletal muscle, as epididymal white adipose tissue (eWAT) and liver REPS1 phosphorylation was not affected by insulin or diet. This was despite lowered insulin-stimulated AKT S473 phosphorylation in all three tissues. Furthermore, the insulin-induced drop in blood glucose levels correlated with skeletal muscle REPS1 S709 phosphorylation levels ($r^2 = 0.69$, $P = 0.01$) (Figure S5A).

To determine if this impairment is present in humans, we analyzed skeletal muscle biopsies from 10 people with T2D and 10 controls matched by age, sex, and BMI with normal glucose tolerance (NGT) in the resting, basal and insulin-stimulated steady-state periods of an hyperinsulinemic euglycemic clamp (Figure 5D). People with T2D exhibited lowered insulin sensitivity than controls ($P < 0.001$) (Figure 5D). REPS1 S709 phosphorylation was increased in response to insulin infusion by 3.5-fold ($P < 0.05$) in the NGT group compared to 2.0-fold in the T2D group ($P = 0.3$)

(Figure 5E). We observed a highly heterogeneous response in both groups. Therefore, we correlated the delta (Post-Pre clamp) response in phosphorylated REPS1 S709 with whole-body insulin sensitivity. Strikingly, there was an interaction in responses between individuals with T2D and NGT (ANCOVA interaction P = 0.024) (Figure 5F). Therefore, we tested individual associations within each group and found correlations for both groups (NGT: r^2=0.65, P = 0.005, T2D: r^2=0.75, P = 0.003) (Figure 5F). Together, these results highlight the role of REPS1 as a key signaling protein impaired in insulin resistance.

REPS1 Variants' Association with Complex Traits, mRNA Expression, and Splicing

After identifying that REPS1 was closely linked to glucose uptake and insulin sensitivity, we explored whether *REPS1* gene variants are associated with cardiometabolic health. By analyzing the NHGRI-EBI Genome-wide association studies (GWAS) catalog, we identified 17 *REPS1* variants linked to 22 distinct phenotypes ($P < 1x10^{-6}$)[53–57]. Using the 1000G European reference panel for linkage disequilibrium (LD)-pruning, we discerned 6 independent *REPS1* signals ($r^2 <$ 0.1). Employing Open Target Genetics, we focused on the lead variant with the most significant associations within each signal (Figure 6, Supplementary Table 2A-B). Remarkably, 4 out of these 6 independent lead variants (rs7870658, rs2750415, rs66883945, and rs62441843) are associated with lipid traits. Two lead variants (rs66883945, rs62441843), located between *REPS1* and *ABRACL*, also share associations with appendicular lean mass, standing height, and sex-hormone binding globulin (SHBG). Intriguingly, two lead variants within *REPS1* introns (rs7870658, rs2750415) are associated with cardiometabolic diseases in type 2 diabetes, such as coronary artery disease and chronic kidney disease. Finally, two other lead variants in *REPS1* introns are singularly associated with corneal-related traits (rs12193050) and leisure screen time (rs200307517), respectively.

To evaluate the association of the 6 independent *REPS1* lead variants with differential expression (eQTL) and alternative splicing (sQTL) of *REPS1* across tissues and cell types, we queried each variant in Open Target Genetics (Figure 6, Supplementary Table 2C). The majority of the associations were linked to altered expression in blood (5/5 lead variants), monocytes (4/5 variants), brain (2/5 variants) and fibroblasts (1/5 variants). However, two lead variants displayed association to muscle tissue: rs12193050 as an eQTL for muscle, and rs2750415 acts as an sQTL for skeletal muscle. This suggests a potential mechanism in which these genetic variants influence muscle-specific gene regulation of *REPS1*.

Discussion

Insulin and exercise potently stimulate glucose uptake in skeletal muscle but the signaling pathways remain largely understudied in clinical material. Here, we mapped the insulin- and exercise-stimulated phosphoproteome of skeletal muscle from the same individuals. We revealed overlapping and unique signaling events triggered by insulin and exercise. REPS1 emerged as a key protein phosphorylated at S709 in response to both exercise and insulin, impacting skeletal muscle glucose uptake. Moreover, phosphorylation of REPS1 strongly correlated with insulin sensitivity and was specifically impaired in skeletal muscle under insulin-resistant conditions, emphasizing its relevance in metabolic diseases such as T2D.

Insulin and exercise induced substantial changes in protein phosphorylation, particularly exercise, which affected 50% of the phosphoproteome. While most of these changes are consistent with previous phosphoproteomic studies[29–31], this study stands out as the first to comprehensively map the deep phosphoproteome in response to an acute insulin- and exercise-stimulation within the same individuals. The study design minimized inter-subject variability and allowed for a precise interrogation of both distinct and shared signaling events induced by these diverse stimuli. This dataset has the potential to serve as a valuable resource for generating novel hypothesis. From our analysis, 71 phosphosites consistently responded to both insulin and exercise, of which some sites potentially affect glucose uptake. We highlight an intriguing (de)phosphorylation event on the protein CLASP2, where both insulin and exercise led to dephosphorylation of the S327 residue and phosphorylation of the S370 residue, close in space in a disordered region. This mechanism was also observed on the sister protein CLASP1 (Site S559 and S600). CLASP2 regulates insulin-stimulated microtubule dynamics, is directly associated with GLUT4, and is required for insulin-stimulated glucose uptake[40,41]. Therefore, CLASP1/2 are likely core proteins required for exercise/insulin-stimulated GLUT4 translocation. Additionally, we also identify vesicle-associated membrane protein-associated protein A (VAPA, also known as VAP-33) was phosphorylated on S214 in response to insulin and exercise. VAPA associates with vesicle-associated membrane protein 2 (VAMP2) and regulates an insulin-dependent insertion of GLUT4 into the plasma membrane[58]. Thus, insulin and exercise stimulate an overlapping set of proteins important for translocation and insertion of GLUT4-vesicles into the plasma membrane.

Our major discovery centers on the phosphorylation of REPS1 on S709 in response to insulin and exercise and the validation of this signal transducer in skeletal muscle glucose uptake. REPS1 was first characterized as a regulator of endocytosis and epidermal growth factor receptor (EGFR) internalization[47,48]. However, in HeLa cells REPS1 knockout is without effect on EGFR

internalization, but transferrin receptor (TfR) recycling is impaired when REPS1 lacks a phosphorylatable S709 site, emphasizing the functional importance of this site[59]. Considering GLUT4's presence in TfR-positive vesicles, which are responsive to insulin[6], we propose that REPS1 plays a role in regulating GLUT4 recycling. Our evidence indicates REPS1 binds to the AP-2 complex and associated kinases (BMP2K, AAK1), suggesting a role in endocytosis, although the specific stage of REPS1 interaction with the endocytic machinery remains unknown. REPS1 forms a complex with RALBP1 in fibroblasts regulating exocytotic processes including trafficking of GLUT4[52]. As we observed a substantial co-enrichment of RALBP1 with REPS1, we interpret this as further evidence for a role in glucose transport via GLUT4 exocytosis in skeletal muscle. Taken together, we propose a dual role for REPS1: 1) sorting of GLUT4 vesicles in early endosome during endocytosis and 2) acute exocytosis processes possibly though interaction with RALBP1/RALA.

Multiple kinases have been implicated in exercise- and insulin-stimulated glucose uptake in skeletal muscle. Here we identify that phosphosites induced by both insulin and exercise are predicted S6K and RSK kinase family substrates. In addition, acute inhibition of RSK blocked insulin-stimulated glucose uptake in skeletal muscle cells and tissue. The role of RSK in glucose uptake is also supported by a direct interaction and phosphorylation of TBC1D4 with RSK in adipocytes[46]. Here RSK1 was required for stress-stimulated glucose uptake. Our findings corroborate a similar axis involving RSK, as we identify RSK as an upstream kinase of REPS1. RSK activation can occur through multiple pathways including the MAPK pathway and by direct phosphorylation by PDK1[60]. In our study, we did not find evidence that PDK1 or the AKT-mTOR-S6K pathway regulate REPS1 S709 phosphorylation in response to insulin stimulation. Instead, we observed REPS1 phosphorylation is regulated via a MEK-ERK-RSK-REPS1 signaling axis. Our study validates REPS1 as a new signaling node downstream of the MAPK-RSK pathway mediating glucose uptake in skeletal muscle.

In humans, we found a strong correlation between insulin-stimulated leg muscle glucose uptake and REPS1 S709 phosphorylation. Notably, 86% of the variance in leg-glucose uptake could be explained by changes in REPS1 S709 phosphorylation. While this does not establish causality, our study provides evidence of impaired insulin-stimulated glucose uptake upon lowering REPS1 expression and S709 phosphorylation in muscle cells, strongly suggesting a direct role of REPS1 in insulin stimulated muscle glucose uptake. However, from the current study, the role of REPS1 in exercise-mediated glucose uptake is less clear. We did not find an association between REPS1 S709 phosphorylation and contraction-mediated glucose uptake in mice. Similarly, exercise-

induced glucose uptake during a one-legged knee extensor exercise did not correlate with levels of REPS1 phosphorylation. Since exercise activates multiple signaling pathways, effects on glucose uptake are likely mediated by various signaling events beyond in addition to just REPS1. Moreover, REPS1 phosphorylation likely plays a crucial role in glucose uptake during recovery after an acute bout of exercise. In addition, REPS1 may play a role in the insulin-sensitizing effects of exercise on GLUT4 trafficking, potentially through endocytosis/vesicle-sorting of GLUT4 into an insulin-responsive compartment.

Insulin-stimulated glucose uptake into peripheral tissues (e.g., muscle, adipose tissue) or inhibition of glucose production (liver) are compromised in the insulin resistant state. Therefore, we hypothesized that insulin-stimulated phosphorylation of REPS1 at S709 would also be affected in these metabolically active tissues. Despite high expression of REPS1 in both the liver and white adipose tissue, insulin-stimulated phosphorylation of REPS1 at S709 was unique to skeletal muscle. This signaling was diminished in skeletal muscle of insulin-resistant mice. Skeletal muscle contains a high expression of GLUT4 and the translocation of GLUT4-containing vesicles to the plasma membrane can be driven by multiple stimuli including muscle contractions[61]. Therefore, a unique signaling pathway that governs GLUT4 plasma membrane translocation in skeletal muscle likely exists.

Translating our findings in mouse to human skeletal muscle, we observed considerable variability in insulin-stimulated REPS1 phosphorylation among individuals with normal glucose tolerance and those with T2D. Interestingly, this variability aligned closely with individual differences in overall insulin sensitivity. This alignment leads us to posit that REPS1 may serve as a pivotal signaling node in humans, holding substantial clinical relevance for metabolic diseases characterized by insulin resistance. In this line, in published GWAS we found that two independent lead variants (rs12193050, rs2750415) were associated with the expression and pre-mRNA-splicing in muscle and skeletal muscle tissue, respectively, implicating potential population heterogeneity in REPS1 (isoform) levels. Several genetic variants were related to lipid traits, lean mass, and T2D-related complications. While we anticipated more associations related to glycemic control, the limited methods for evaluating skeletal muscle insulin sensitivity might be a contributing factor. Comprehensive GWAS studies employing hyperinsulinemic clamp techniques are essential, as they could reveal previously undetected associations within genes like *REPS1*, providing a more detailed picture of muscle insulin sensitivity.

In conclusion, we mapped a comprehensive insulin and exercise-induced phosphoproteome in skeletal muscle from healthy individuals. We identified a total of 233 phosphorylation events

shared between the two stimuli with 71 residues on 55 proteins regulated in the same direction, and many of which have a role in vesicle trafficking. We provide a comprehensive resource for future studies investigating the role of protein phosphorylation on skeletal muscle glucose uptake and metabolism. We highlight the conserved S709 residue of REPS1 as an insulin and exercise signaling convergence point in mouse and humans and demonstrate a tight association between this phosphorylation site and insulin-stimulated skeletal muscle glucose uptake. REPS1 binding partners and the putative upstream kinase, RSK, suggest a dual role in endocytosis and exocytosis regulation. The skeletal muscle-tissue specific insulin response and impairment in insulin resistant mice and humans emphasize the clinical relevance of REPS1 as a potential therapeutic target for diseases characterized with insulin resistance, such as T2D.

Limitations of study

The participants recruited for the phosphoproteome study were all young healthy men, who do not represent overall population heterogeneity including differences in sex, age, BMI and ancestry. This initial focus allowed us to control for these factors and uncover novel insights into insulin and exercise biology

We provide initial evidence that REPS1 is phosphorylated in response to insulin and exercise; however, further studies are needed to elucidate the precise role of REPS1 phosphorylation in contraction-mediated glucose uptake and exercise. Future work should also explore its the involvement of REPS1 during recovery from exercise and how this may enhance insulin sensitivity. Furthermore, additional studies to determine the time course and dose dependent response of insulin- or exercise-induced REPS1 phosphorylation are warranted.

The exact mechanistic interplay between REPS1's endocytotic and exocytotic functions remains to be fully understood. Investigating these pathways in more detail could provide new insights into REPS1's broader role in cellular regulation. While our findings emphasize the importance of the RSK-REPS1 axis, other regulatory inputs, including alternative kinases and phosphatases, may also influence REPS1 function and should further explored

Methods

Subjects and eligibility criteria

Eight healthy male volunteers took part in the study and were selected from a sub-group of a larger study[62]. Prior to inclusion, subjects met for an assessment of eligibility criteria. The criteria were: healthy males, 18–36 years of age, non-smoker, engaged in physical activity for 2–5

h/week, exhibit maximum oxygen uptake (40–60 ml/kg/min, lean mass 55–65 kg or lean mass index 14–22 kg/m^2, no usage of beta2-agonists or other prescription medicine, and no allergy towards study medication. Withdrawal criteria included experiencing unacceptable side effects, complications related to the study, or non-compliance with the protocol. The study adhered to the 2013 Helsinki Declaration and was approved by the ethics committee of Copenhagen, Denmark (H-4-2014-002). All subjects provided oral and written informed consent before being included in the study. Body composition was assessed by dual-energy X-ray absorptiometry (Lunar DPX IQ, Version 4.7 E, Lunar Corporation, Madison, WI, USA) (DXA) followed by incremental cycling to exhaustion on a bike ergometer for assessment of VO2max by indirect calorimetry (Monark LC4, Monark Exercise AB, Vansbro, Sweden) as previously described[63].

Hyperinsulinemic euglycemic clamp trial

Subjects arrived at the laboratory in a fasting state for assessment of insulin-stimulated whole-body glucose disposal during a hyperinsulinemic-euglycemic clamp. They refrained from vigorous physical activity and alcohol for 48 h and caffeine and nicotine for 24 h. Before the clamp, subjects ingested four to five potassium tablets to prevent hypokalaemia (Kaleorid, 750 mg KCl, Karo Pharma, Sweden) and had a catheter placed in the antecubital vein for infusion of glucose and insulin. In addition, catheters were inserted in the femoral vein and artery and a muscle biopsy was sampled during local anesthesia. The clamp was initiated with a 1 min priming dose of 53.5 pmol/kgbw insulin (100 IU/ml, Novo Nordisk, Copenhagen, Denmark) and continued for 120 min with a constant insulin infusion of 8 pmol/kgbw/min. Femoral venous and artery blood samples were collected before the clamp and every 5 min during the clamp for assessment of glucose concentration. Furthermore, blood samples were collected before and during the clamp for determination of plasma insulin. Glucose was infused during the clamp from a 20% glucose solution (Fresenius Kabi, 200 mg/ml) to maintain euglycaemia at □5 mM. At the end of the clamp, another muscle biopsy was sampled.

Cycle exercise trial

On a separate day in a fasting state, a resting muscle biopsy was obtained under local anaesthesia (2 ml lidocaine without noradrenaline (epinephrine), Xylocaine 20 mg/ml, AstraZeneca, Cambridge, UK). Hereafter, subjects completed 10-min bike ergometer exercise with highest possible effort. Immediately, after the exercise, another biopsy was sampled. Hyperinsulinemic-euglycemic clamp trial and the exercise trials (in same eight individuals) were separated by wash out period of around 1-2 weeks.

Blood analyses

Blood samples were drawn in EDTA tubes and stored on ice for 30 minutes before they were spun at 4°C and 3000 rpm for 5 minutes, after which plasma was collected and stored at 80°C until analysis for catecholamines, insulin, and FFAs. Plasma adrenaline and noradrenaline were determined with a commercially available ELISA kit (2-CAT plasma ELISA high sensitivity kit; Labor Diagnostica Nord, Nordhorn, Denmark) according to the manufacturer's instructions. Plasma insulin was determined with ELISA (Dako Denmark) according to manufacturer's instructions. Plasma FFA was determined with ELISA (NEFA-HR, R1 and R2 sets; TriChem ApS–Interkemi, Skanderborg, Denmark) according to the manufacturer's instructions.

One-legged knee extensor exercise

Participants met in the morning after an overnight fast. Upon arrival at the laboratory, subjects rested in a supine position and catheters were inserted into the femoral artery and vein during local anesthesia (20 mg/mL lidocaine without adrenaline, Xylocaine; AstraZeneca, London, UK). Incisions were made through the skin and fascia at the belly of the vastus lateralis muscle for sampling of biopsies. After 30 min of rest in a sitting position, participants were moved to a knee extensor ergometer[64], where their right foot was strapped to a boot that was connected to the ergometer crank. Participants then performed a brief warmup, followed by a bout of exercise at 90% of maximal incremental peak power output until exhaustion. During exercise, participants were instructed to contract during the concentric phase of movement while relaxing during the eccentric phase to minimize involvement of hamstring muscles. Participants maintained a cadence of 60 RPM and exhaustion was defined as inability to maintain 60 RPM for >5 s during strong verbal encouragement.

Femoral arterial and venous blood samples were drawn before exercise, immediately following exhaustion, and 1-10 min in recovery. Samples were drawn in heparinised tubes for immediate analyses of glucose using an ABL800 Flex (Radiometer, Copenhagen, Denmark). Femoral artery blood flow was measured at the same time as blood sample collection by ultrasound Doppler (Logic E9, GE Healthcare, Illinois, US) equipped with a linear probe operating with imaging frequency of 9 MHz and Doppler frequency of 4.2–5.0 MHz. The site of blood velocity measurements was at the common femoral artery below the inguinal ligament but above the bifurcation to the superficial and profound branches to avoid turbulence from the bifurcation. Doppler traces were recorded and averaged over 10 s with the midpoint of the sampling period being the time of blood sampling.

A muscle biopsy was sampled from the vastus lateralis using the Bergström needle procedure[65] before and immediately following exercise.

T2D study

A subset of 10 patients with type 2 diabetes from the "specialist supervised individualized multifactorial treatment of new clinically diagnosed type 2 diabetes in general practice (IDA)" study[66] and 10 persons with normal glucose-tolerance matched on sex, BMI, age and smoking took part in the T2D study. Informed consent was obtained from all subjects before participation. The study was approved by the Regional Scientific Ethical Committees for Southern Denmark (Projekt-ID: S-20120186) and was performed in accordance with the Helsinki Declaration.

All participants had normal results on blood screening tests and ECG. An HEC was performed after an overnight fast. The participants were instructed to refrain from physical activity 48 h prior to test. In patients with T2D, glucose, lipid and blood pressure lowering medication was withdrawn one week prior to the clamp studies. In brief, the clamp consisted of a 2-hour basal period with infusion of a primed constant amount of [3-3H]-tritiated glucose to obtain tracer equilibration. This was followed by a 4-hour insulin-stimulated period using an insulin infusion rate of (40 mU · m-2 · min-1) to achieve euglycemia (5,0-5,5 mmol/l) in the insulin-stimulated steady-state period. Skeletal muscle biopsies were obtained before and after the insulin infusion period under local anaesthesia (lidocaine).

Muscle biopsies

All skeletal muscle biopsies were sampled using the suction-modified Bergström needle technique[65]. This technique is widely used because it is safe, minimally invasive, and provides adequate material for biochemical analyses (typically 100-150 mgwet wt) [67]. Before sampling, we applied local anesthesia (2-3 mL lidocaine without epinephrine, Xylocaine, 20 mg/mL, AstraZeneca, Cambridge, UK) through the skin at the belly of the vastus lateralis muscle. Next, we made a small incision (3 mm) and nicked the muscle fascia using a sterile surgical blade. Through this incision, we collected the biopsy using a 4-mm Bergström needle (Stille, Stockholm, Sweden) with suction. Immediately after sampling, we washed the biopsy in sterile saline solution (0.9% NaCl, Fresenius Kabi, Sweden) and quickly removed visible blood, connective tissue, and fat after which we froze the sample in liquid nitrogen and stored it at –80°C until analysis.

Sample processing & phosphoproteomics

Freeze-dried muscle was powdered and lysed in 4% sodium dodecyl sulfate (SDS), 100mM Tris pH=8.5 with an Ultra Turrax homogenizer (IKA). Samples were immediately boiled for five minutes, tip-probe sonicated and spun down at 16,000g for 10 minutes. The resultant supernatant was protein precipitated using four times the volume of -20°C acetone overnight. The protein pellets were washed 3 times in acetone, air-dried and resolubilized in 4% sodium deoxycholate (SDC), 100mM Tris pH=8.5 with a bioruptor sonicator (30s on/off, 15 cycles). Protein concentration was determined using Bicinchoninic acid (BCA) assay and 1mg of protein was subsequently reduced and alkylated for 5 minutes at 40° Celsius with 5mM tris-(2-carboxyethyl)phosphine (TCEP) and 40mM 2-chloroacetamide (CAA), respectively. Enzymatic digestion was initiated by adding Trypsin and lysC at a 1:100 enzyme:protein ratio and the mixture was digested overnight at 37°C. Protein digestion was stopped by adding 1% trifluoroacetic acid (TFA) and precipitate was cleared by centrifugation at 20,000g for 10 minutes. Supernatant was desalted on C18 cartridges (Sep-Pak, waters) and eluted with 50% acetonitrile (ACN). Peptides were then vacuum dried and concentration was determined by measuring the absorbance at 280/260 (NanoDrop, Thermo Scientific). 200µg of peptides in 100mM HEPES pH=8-5 were then labeled with 400µg of 11-plex TMT (Thermo, #A34808) for one hour followed by 15 minutes of quenching with 0.27% NH2OH. Peptides pre/post exercise (study day 1) or insulin (study day 2) were labeled on two separate 11-TMT-plexes. A pool of peptides across conditions were placed in the last channel 131C. An aliquot of each sample was tested for near-complete labeling efficiency (>99% labeling).

TMT-peptide pools were then desalted on C18 cartridges and eluted with 50% ACN. Prior to phospho-enrichment, the samples were adjusted to 6% TFA, 3mM KH2PO4, and 50% ACN. TiO□-beads (GLsciences) were equilibrated in 80% ACN and 6% TFA. Equilibrated TiO□-beads were added in a ratio of 12:1 (bead to peptide) for 15 minutes rotating end-over-end at room temperature. Supernatant was passed through a second and third round of enrichment in an 8:1 and 4:1 bead to peptide ratio, respectively. Beads were combined and washed four times in 60% ACN and 1%TFA. Beads were then transferred in 80% ACN and 0.5% acetic acid on top of 2xC8 layer plugged into a p200 tip. Captured phosphopeptides were then eluted in 80% ACN, 1.25% NH4OH and vacuum dried for 20 minutes. 1% TFA was added to the samples and loaded on to equilibrated three layered Styrene-DivinylBenzene – Reversed Phase Sulfonate (SDB-RPS) StageTips. The phosphopeptides were subsequently washed in 1% TFA in isopropanol followed by two washes with 0.2% TFA. Lastly, phosphopeptides were eluted in 80% ACN and 1.25% NH4OH, vacuum dried and resuspended in 20uL 5% ACN and 0.1% TFA.

Immunoprecipitation and interactome analysis

Upon C2C12 myoblast differentiation, cells were transduced with 100,000 virus per well for 48 hours before media change. On day of harvesting, cells were starved for three hours and lysed in ice-cold lysis buffer (1% triton-x100, 150mM NaCl, 50mM Tris pH=7.4, 1mM EDTA, 6mM EGTA) supplemented with protease and phosphatase inhibitors (Roche). Cell homogenate was incubated end-over-end for 45 minutes before centrifugation at 16,000G for 10 minutes at 4°C. Protein concentration was determined by the BCA assay. A total of 200µg of protein lysate per sample was used for either FLAG- or endogenous IP. For IP, appropriate antibody was added to lysate and left overnight. The following day protein-G agarose beads were added and samples incubated for two hours. Beads were washed two times in lysis buffer followed by two washes in 150mM NaCl, 50mM Tris pH=7.4. Proteins were then eluted, reduced and alkylated from beads in 2M Urea, 1mM dithiothreitol (DTT) and 0.5µg trypsin for one hour. Supernatant was collected and alkylated with 5mM 2-Iodoacetamide (IAA) and digested overnight at 37°C. The following day, digestion was stopped by adding 1% TFA and 20% of eluate was loaded onto equilibrated Evotips ready for measurement.

LC-MS measurements for phosphoproteome analysis

Desalted and TMT11plex-labeled peptides were resuspended in buffer A* (2% ACN, 0.1% TFA), and fractionated into 16 fractions by high-pH fractionation. In short, 4µg of peptides were loaded onto a 30 cm x 0.25mm Pepsep 1.9um ReproSil C18 120 Å column via an EASY-nLC 1200 HPLC (Thermo Fisher Scientific) in Spider buffer A (1% tetraethylammonium fluoride (TEAF), 0.1% tetraethylammonium (TEA)). Peptide separation was done with a non-linear gradient of 5 – 44 % Spider buffer B (1% TEAF, 0.1% TEA, 80% ACN) at a flow rate of 1.5 µL / min over 62 min. Collection of fractions was done at 60 s interval with a concatenation workflow to achieve a total of 16 fractions. All fractions were then evaporated, and peptides resuspended in buffer A*, and measured using an EASY-nLC 1200 HPLC system (Thermo Fisher Scientific) coupled through a nano-electrospray source to a Tribrid Eclipse mass spectrometer (Thermo Fisher Scientific). Peptides were loaded in buffer A (0.1 % formic acid (FA)) and separated on a 25 cm column Aurora Gen1 (kept at 50° C), 1.6uM C18 stationary phase (IonOpticks) with a non-linear gradient of 5 – 44% buffer B (0.1% FA, 80% ACN) at a flow rate of 400 nL/min over 91 min with a total gradient time of 101 min including washing. Spray voltage was set to 2400 V. Data acquisition switched between a full scan (120K resolution, 50ms max. injection time, AGC target 100 %) and 3 seconds cycle time-controlled data-dependent MS/MS scans (50K resolution, 120ms max. injection time, AGC target 200 % and HCD activation type). Isolation window and normalized

collision energy were set to 0.7 and 35, respectively. Precursors were filtered by charge state of 2-6 and multiple sequencing of peptides was minimized by excluding the selected peptide candidates for 45 s. The PrecursorFit filter, Fit error 70% in a window of 1.2Da, was also activated.

LCMS measurements for interactome analysis

For the interactome experiment, the peptides were subjected to separation using a 15 cm column with an internal diameter of 150 µM, which was packed with 1.9 µm C18 beads (Pepsep brand). This separation process was carried out on an Evosep ONE HPLC system, employing the specific protocol designed for '30 samples per day', and peptides were introduced into the system via a CaptiveSpray source equipped with a 20 µm emitter. The mass spectrometric analysis was performed using a timsTOF SCP mass spectrometer from Bruker, functioning in the parallel accumulation-serial fragmentation (PASEF) mode[68]. To elaborate, the DDA-PASEF scan for both MS and MS/MS was configured to encompass a range from 100 to 1700 m/z. The TIMS mobility spectrum was set within the bounds of 0.6 to 1.6 (V cm−2). Both TIMS ramp and accumulation times were precisely fixed at 100 ms. During each cycle, which lasted a total of 1.17 seconds, 10 PASEF ramps were recorded. The MS/MS target intensity was defined at 20,000, with an intensity threshold at 1,000. Furthermore, a stringent exclusion list was applied, set at 0.4 min for precursors within a narrow window of 0.015 m/z and 0.015 V cm−2.

Data analysis

Raw files were quantified in MaxQuant v2.0.1.0 against the reviewed human fasta (09082021)[69]. Default settings were applied including a minimum peptide length of seven amino acids. Deamidation (NQ), methionine-oxidation (M) and N-terminal acetylation were set as fixed modifications. Phospho (STY) was set as a variable modification. For interactome analysis, raw files were processed in Fragpipe (v.20.0) with default settings and MaxLFQ enabled[70].

Bioinformatics analysis

Maxquant output STY-file was imported into Perseus (2.0.7.0)[71] and phosphopeptides expanded to represent phosphosites. Data was then imported into R studio v4.2.1 and log2-transformed. Data were median-scaled and unwanted variation was removed by normalizing to stably phosphorylated sites with the phosR package[72]. The data were filtered to have no missing values. To identify differentially regulated phosphosites, we applied limma with ebayes data smoothening[73]. The linear model was blocked for subjects. *P* values were adjusted with the

Benjamini Hochberg (BH) method and adjusted *P* values < 0.05 were considered statistically significant.

Kinase-activation analysis for Ser/Thr kinase was performed by the online tool: https://kinase-library.phosphosite.org/site[34]. Sequence windows were uploaded with phosphorylated residue centralized. Kinases were then filtered to be expressed in human skeletal muscle as part of the human protein atlas database (~13000 transcripts)[35]. Regulatory- and disease-associated sites were downloaded from PhosphositesPlus[74]. For each subcategory a two-sided fishers exact test was applied.

Go enrichment analysis

Gene-ontology enrichment analysis was done with the clusterProfiler package[75]. Enrichment was done on the gene-level. Whole phosphoproteome and interactome data was used as background. BH adjusted *P* values < 0.05 were considered significant.

Alphafold-structure

Predicted 3-dimensional structure of CLASP2 was extracted from alphafold and specific phosphorylated residues were edited in the Pymol software[76].

Interactome data analysis

The combined_protein output file was imported into R studio. Data were log2-transformed and filtered for quantification in at least 50% (3 samples) within a group. Missing values were imputed from a normal distribution with a mean downshift of 1.8 and standard deviation of 0.3. A two-sided t-test was used to assess differences between groups. BH adjusted *P* values < 0.05 were considered significant.

Querying genetic associations of REPS1 variants

To identify which traits are associated with the *REPS1* gene, we searched for associations between *REPS1* variants and complex traits and diseases in genome-wide association studies (GWAS) by querying "*REPS1*" in the NHGRI-EBI GWAS catalogue[53] on October 2, 2023. To assess whether the reported associations belong to independent signals, we computed a linkage disequilibrium (LD) matrix using the LDLinkR package (v1.4.2)[54,55]. We considered that variants represent independent signals if the r^2 between the variants was <0.1 within ±500kb. For each independent signal, we identified the lead variant with the lowest *P* value and queried it in Open Target Genetics[57] to obtain additional associations from a different source ($P < 1x10^{-6}$). We also

assessed whether these variants were significantly associated with the mRNA expression (eQTL) or splicing (sQTL) of *REPS1* across different tissues by querying Open Target Genetics using otargen R package (v.1.0.0)[77].

Animal experiments

All animal experiments were approved by the Danish Animal Experiments Inspectorate (License no. 2017-15-0201-01276 & 2018-15-0201-01493). 7-week old C57BL/6NTac male mice were fed *ad libitum* a LFD (Research diet:D12450Ji) or HFD diet (Research Diet:D12451i) for 16 weeks on a normal 12:12-h light dark cycle. On the day of termination, fed mice were anaesthetized by an intra-peritoneal injection of pentobarbital (10mg/100mL) and injected retro-orbitally with either saline or human insulin (1U/kg). After 15 minutes, tissues were immediately removed and frozen in liquid nitrogen until further analysis. Blood glucose levels were measured pre/post saline/insulin injection by a glucometer.

In situ contractions

Mice (male, C57BL/6NTac; 12-16 weeks of age) were anesthetized with pentobarbital (2.5 mg/mouse) and kept warm on a heating mat throughout the experiment. The sciatic nerve was exposed and stimulated (0.5 s train every 1.5s at 5V, 0.1ms, 100hz) to contract the lower leg muscles. The contralateral leg to the contracted leg was sham operated and serves as a non-contracted control. A retro-orbital injection was administered immediately prior to nerve stimulation (15 mU insulin or saline, 3 mg glucose, 20 uCi [3H]2-deoxyglucose in gelofusine) and tissues were dissected 15 minutes after glucose tracer, insulin/saline injection and the initiation of contraction. The TA muscle was quickly dissected and snap frozen. Muscles were processed as in[78]. Protein concentration was determined by the BCA-assay (Thermo #23225). Muscle protein lysate was mix with either 0.3M $Ba(OH)_2$ and $ZnSO_4$ or 4.5% $HClO_4$ before centrifugation at 10000 RPM for 5 minutes at room temperature. Supernatant was collected and added to scintillation vials with Ultima Gold scintillation fluid (Perkin Elmer #6013329) before counted on a Hidex 300 SL scintillation counter. Blood was collected every 5 minutes and specific activity calculated as in[78].

Ex-vivo muscle insulin stimulated glucose uptake

Soleus muscle was rapidly dissected, as previously described[79,80], and incubated into warmed (30ºC) and oxygenated (95% O_2, 5% CO_2) Krebs-Ringer buffer (KRB, 117 mM NaCl, 4.7 mM KCl, 2.5 mM CaCl2, 1.2 mM KH2PO4, 1.2 mM MgSO4, 24.6 mM NaHCO3) with 0.1% bovine serum

albumin (BSA), and 5 mM glucose in a myograph system (820MS DT, Denmark). Muscles were pre-incubated for 60 minutes in KRB containing BSA, 8mM mannitol, and 2mM pyruvate 10uM BI-D1870 or vehicle (DMSO). The media was then changed for a 30 minute incubation with insulin (300µIU/ml, Actrapid, Novo Nordisk, Denmark). After 20 min, the buffer was changed to a buffer containing 1 mM of 2-DG and 3H-2-DG (0.0185 MBq/mL, PerkinElmer, #NET549A005MC), 7 mM of mannitol and 14C-mannitol (0.0167 MBq/mL, PerkinElmer, #NEC314250UC) for 10 minutes. After which, muscles were harvested and snap frozen in liquid nitrogen. Muscles were processed as above and supernatant protein lysate counted on a Hidex 300 SL scintillation counter. All muscle counts were related to the specific activity in each myograph chamber.

Cell culture

C2C12 cells were cultured in Dulbecco´s Modified Eagle Medium (DMEM #41965-039) supplemented with 10% Fetal Bovine Serum and 1% penicillin streptomycin (P/S). Cells were maintained in an incubator with 37ºC and 5% CO_2. C2C12 myoblasts were grown to ~80% confluence before initiating differentiation with DMEM supplemented with 2% Horse serum and 1% P/S.

Signaling experiments: C2C12 myotubes were serum-starved for 4 hours before pre-incubating cells with inhibitors (10µM BI-D1870, 10µM U0126, 100nM Rapamycin, 10µM PF-4708671 and 10µM MP-7) for 20 minutes followed by 10 minutes stimulation of 100nM insulin. Cells were then washed twice in ice-cold phosphate buffered saline (PBS) and lysed in 2% SDS, 50mM Tris pH = 7.4. Lysate was then boiled for 5 minutes at 95°C. A small aliquot was used for DC assay protein determination. Sample concentration was adjusted with SDS-buffer and 4x sample buffer (10% 2-mercaptoethanol, 13.3% glycerol and 444mM Tris-HCl pH=6.8).

SiRNA-mediated knockdown: On the same day as differentiation was initiated, cells were transfected with siRNA against *Reps1* (Dharmacon #L-040836-01-0005) or scramble siRNA (Dharmacon #D-001810-10-20). Complexes of Transit-X2 (Mirus #MIR6000), Opti-MEM and siRNA were prepared in a concentration of 25nM and incubated at room temperature for 20 minutes before the siRNA complexes were added to the cells. The culture media was changed every ~48 hours. Knockdown of *Reps1* was later confirmed by Western Blot.

Aav transduction: Mouse *Reps1* (NM_009048.2, VectorBuilder) with N-terminal FLAG tag was subcloned into Aav serotype 1 vector under a CMV promoter. The control-FLAG contained a random open-reading frame stuffer similarly under a CMV promoter. Vectors were added at a

concentration of 10x10^5 per well in a 6-well plate at day of differentiation induction. The culture media was changed every ~48 hours.

Glucose uptake assay

Glucose uptake of C2C12 myotubes was measured with a ^{3}H-2-Deoxyglucose (2DG) assay on day 6 of differentiation. Cells were serum starved for 4 hours in serum free DMEM with 1% P/S prior to the assay. After serum starvation cells were washed one time in pre-warmed Krebs Ringer HEPES buffer (140 mM NaCl, 4.7 mM KCl, 2.5 mM, 1.25 mM, 1.2 mM HEPES, 0.2% bovine serum albumin (BSA), pH=7.4) before incubation with KRHepes or 100 nM insulin for 30 minutes. Thereafter, cells were incubated for 5 minutes with ^{3}H-2DG (0.4µCi/mL) and 50µM 2DG. Glucose uptake was stopped by washing cells with ice cold KRHepes buffer while the plate was on ice. Cells were then lysed in 2 % SDS and boiled for 5 minutes at 95ºC. 100 µL cell lysate was added to 3 mL of Ultima Gold scintillation liquid (Perkin Elmer #6013329). Samples were kept in the dark overnight and ^{3}H-2DG uptake was measured the following day on a Hidex 300 SL scintillation counter. ^{3}H-2DG uptake was subsequently adjusted for protein content using a detergent compatible (DC)-assay (Bio-Rad). The glucose-uptake experiment was repeated on three separate days with same observed effect. For the RSK-inhibitor glucose uptake experiment, cells were preincubated with 10 µM BI-D1870 for 20 minutes before 10 minutes of 100nM insulin stimulation.

GLUT4-translocation assay

L6 muscle cells stably transduced with myc-GLUT4 were grown in αMEM medium containing 1% P/S, 10% FBS, and 2µ/mL blasticidin until they reached 70% confluency. The cells were then seeded into a 96-well plate (10,000 cells/well), and differentiation was initiated on the day of confluency in medium with 1% P/S and 2% FBS. On the day of the experiment (day 6), differentiated myotubes were serum-starved for 2 hours. Cells were pre-incubated with either DMSO or 10 µM BI-D1870 for 20 minutes, followed by stimulation with 100 nM insulin for 10 minutes. After treatment, the cells were immediately placed on ice and washed twice with ice-cold PBS before being fixed with 3% paraformaldehyde for 10 minutes. Fixation was quenched using 0.1 mM glycine for 5 minutes, followed by three washes with PBS+ (PBS containing 0.9 mM Ca^{2+} and 0.49 mM Mg^{2+}). The cells were blocked with 5% milk for 10 minutes and then incubated with the primary anti-myc antibody (Sigma-Aldrich #C3956, 1:1000 in 5% milk) for 60 minutes at room temperature. After five washes with PBS+, the cells were incubated with HRP-conjugated goat anti-rabbit antibody (1:1000 in 5% milk, Bio-Rad: #1706515) for 30 minutes, followed by five

additional washes with PBS+. One OPD tablet (Sigma-Aldrich #5412) was dissolved in 0.05 M phosphate/citrate buffer (pH = 5), supplemented with H_2O_2, and added to the cells for 30 minutes in the dark. Absorbance was measured spectrophotometrically at 450 nm using a Hidex plate reader. Cells incubated without the primary antibody were used as controls to subtract background noise. The GLUT4-translocation experiment was repeated on three separate days, consistently showing the same effect.

Immunoblot analysis

WB of animal LFD/HFD tissues: Tissues were powdered and lysed in 4% SDS, 100mM Tris pH=7.4 with an Ultra Turrax homogenizer (IKA) and immediately boiled. Samples were tip-probe sonicated and centrifuged at 16,000g for 10 minutes. Supernatant was collected and protein concentration determined by the DC-assay. 4x Sample-buffer (10% 2-mercaptoethanol, 13.3% glycerol and 444mM Tris-HCl pH=6.8) was added to lysate and boiled again for 5 minutes at 95°C.

WB of human samples: Powdered muscle was lysed in ice-cold homogenization buffer (10% glycerol, 20 mM Na-pyrophosphate, 150 mM NaCl, 50 mM HEPES (pH 7.5), 1% Igepal, 20 mM β-glycerophosphate, 2 mM Na3VO4, 10 mM NaF, 2 mM phenylmethylsulfonyl fluoride (PMSF), 1 mM ethylenediaminetetraacetic acid (EDTA) (pH 8), 1 mM ethylene glycol-bis(β-aminoethyl)-N,N,N,N-tetraacetic acid (EGTA) (pH 8), 10 $\mu g \cdot ml^{-1}$ Aprotinin, 10 $\mu g \cdot ml^{-1}$ Leupeptin and 3 mM Benzamidine) with steel beads at 28.5 Hz for 1 min (Qiagen TissueLyser II, Retsch GmbH, Haan, Germany). Homogenate was then incubated for 1 hour end-over-end at 4°C followed by centrifugation for 20 minutes at 18,320g and 4°C. Protein concentration was determined by the BCA assay.

15µg was loaded on a 4-20% acrylamide gradient gel with 18 or 26-wells (Bio-Rad #5671094 & Bio-Rad #5671095) and separated for 20min at 100v followed by 150V for 1 hour. Proteins were transferred with a semi-dry transfer system (Bio-Rad) onto a polyvinedylene difluoride (PVDF)-equilibrated membrane (Bio-Rad turbo-transfer #1704157) for 7 min at 25V. Membranes were blocked in either 2% milk or 3% BSA in Tris-buffered saline (TBS, pH7.4) supplemented with 0.05% tween-20 for 1 hour and incubated overnight with primary antibody on a rocking platform. The following day, membranes were washed 3 times in TBS-T and incubated for 45 minutes with secondary antibody (Bio-Rad: Goat Anti-rabbit #1706515 or Goat-anti mouse #1706516). Lastly, membranes were washed 3x every 10 minutes for a total of 3 times before ECL (Millipore #WBLUF0500) was added and imaged by chemidoc+ system (Bio-Rad). Immunoblots were analyzed in ImageLab software.

Antibodies:

REPS1 (CST #6404), p-REPS S709 (CST #12005), GAPDH (CST #2118), p-CREB S133 (CST #9198), p-AKT T308 (CST #9275), p-AKT S473 (CST #9271), AKT2 (CST #3063), pan-AKT total (CST #9272), p-ERK1/2 T202/Y204 (CST #9101), ERK1/2 (CST #4696), mTOR (CST #2972), p-mTOR S2448 (CST #2971), p-AMPK T172(CST #2531), AMPKα2 (CST #2532), ACC (CST #3676), p-P70S6K T389 (CST# 9205), P70S6K (CST #2708), p-RPS6 S235/236 (CST #2211), RPS6 (CST #2217), ACTIN (sigma A2066), p-ACC S221 (Millipore 07-303), GLUT4 (Thermo PA1-1065), FLAG (sigma, F7425).

Statistical analysis:

For analysis of paired human samples a two-sided paired samples t-test was used. For two-factor designs a two-way ANOVA analysis was used with or without repeated measures. Tukeys or Sidak multiple comparison test were used as post hoc test dependent on repeated measures. For unpaired two condition design a two-sided two sample t-test was used. Pearson's correlation was used to analyze association between two independent variables (normality tested with the Shapiro-Wilk test $P > 0.05$). In figure 5F, an ANCOVA model was used to predict GIR (dependent variable) by Group (NGT/T2D) and delta (post-pre clamp) p-REPS1 levels (independent variables). Additionally, the model included an interaction term to examine the potential differential effect of p-REPS1 levels on GIR across the two groups (NGT/T2D). P values < 0.05 were considered significant.

Data availability

The mass spectrometry proteomics data have been deposited at ProteomeXchange (http://proteomecentral.proteomexchange.org) via the PRIDE partner repository with the dataset identifier PXD046755, **Username:** reviewer_pxd046755@ebi.ac.uk, **Password:** tn8nQfaa.

References

1. DeFronzo, R. A. *et al.* The Effect of Insulin on the Disposal of Intravenous Glucose: Results from Indirect Calorimetry and Hepatic and Femoral Venous Catheterization. *Diabetes* **30**, 1000–1007 (1981).

2. DeFronzo, R. A., Gunnarsson, R., Bjorkman, O., Olsson, M. & Wahren, J. Effects of insulin on peripheral and splanchnic glucose metabolism in noninsulin-dependent (type II) diabetes mellitus. *J Clin Invest* **76**, 149–155 (1985).

3. McConell, G. K. *et al.* Insulin-induced membrane permeability to glucose in human muscles at rest and following exercise. *J Physiol* **598**, 303–315 (2020).

4. Fueger, P. T. *et al.* Control of muscle glucose uptake: test of the rate-limiting step paradigm in conscious, unrestrained mice. *J Physiol* **562**, 925 (2005).

5. Zisman, A. *et al.* Targeted disruption of the glucose transporter 4 selectively in muscle causes insulin resistance and glucose intolerance. *Nat Med* **6**, 924–928 (2000).

6. Ploug, T., Van Deurs, B., Ai, H., Cushman, S. W. & Ralston, E. Analysis of GLUT4 distribution in whole skeletal muscle fibers: Identification of distinct storage compartments that are recruited by insulin and muscle contractions. *Journal of Cell Biology* **142**, 1429–1446 (1998).

7. Kennedy, J. W. *et al.* Acute exercise induces GLUT4 translocation in skeletal muscle of normal human subjects and subjects with type 2 diabetes. *Diabetes* **48**, 1192–1197 (1999).

8. Kjøbsted, R. *et al.* Intact regulation of the AMPK signaling network in response to exercise and insulin in skeletal muscle of male patients with type 2 diabetes: Illumination of AMPK activation in recovery from exercise. *Diabetes* (2016) doi:10.2337/db15-1034.

9. Karlsson, H. K. R. *et al.* Insulin-Stimulated Phosphorylation of the Akt Substrate AS160 Is Impaired in Skeletal Muscle of Type 2 Diabetic Subjects. *Diabetes* **54**, 1692–1697 (2005).

10. Björnholm, M., Kawano, Y., Lehtihet, M. & Zierath, J. R. Insulin receptor substrate-1 phosphorylation and phosphatidylinositol 3-kinase activity in skeletal muscle from NIDDM subjects after in vivo insulin stimulation. *Diabetes* **46**, 524–527 (1997).

11. Sakamoto, K. *et al.* Role of Akt2 in contraction-stimulated cell signaling and glucose uptake in skeletal muscle. *Am J Physiol Endocrinol Metab* **291**, 1031–1037 (2006).

12. Wojtaszewski, J. F. P. *et al.* Exercise modulates postreceptor insulin signaling and glucose transport in muscle-specific insulin receptor knockout mice. *Journal of Clinical Investigation* (1999) doi:10.1172/JCI7961.

13. Sylow, L. *et al.* Rac1 signaling is required for insulin-stimulated glucose uptake and is dysregulated in insulin-resistant murine and human skeletal muscle. *Diabetes* (2013) doi:10.2337/db12-1148.

14. Park, D. R., Park, K. H., Kim, B. J., Yoon, C. S. & Kim, U. H. Exercise Ameliorates Insulin Resistance via Ca2+ Signals Distinct From Those of Insulin for GLUT4 Translocation in Skeletal Muscles. *Diabetes* **64**, 1224–1234 (2015).

15. Chambers, M. A., Moylan, J. S., Smith, J. D., Goodyear, L. J. & Reid, M. B. Stretch-stimulated glucose uptake in skeletal muscle is mediated by reactive oxygen species and p38 MAP-kinase. *J Physiol* **587**, 3363 (2009).

16. Jensen, T. E. *et al.* Contraction-stimulated glucose transport in muscle is controlled by AMPK and mechanical stress but not sarcoplasmatic reticulum Ca 2+ release. *Mol Metab* (2014) doi:10.1016/j.molmet.2014.07.005.

17. Witczak, C. A. *et al.* CaMKII regulates contraction- but not insulin-induced glucose uptake in mouse skeletal muscle. *Am J Physiol Endocrinol Metab* **298**, 1150–1160 (2010).

18. Henríquez-Olguin, C. *et al.* Cytosolic ROS production by NADPH oxidase 2 regulates muscle glucose uptake during exercise. *Nat Commun* **10**, (2019).

19. Benninghoff, T. *et al.* The rabgaps tbc1d1 and tbc1d4 control uptake of long-chain fatty acids into skeletal muscle via fatty acid transporter SLC27A4/FATP4. *Diabetes* (2020) doi:10.2337/db20-0180.

20. Chadt, A. *et al.* Deletion of both rab-GTPase-activating proteins TBC1D1 and TBC1D4 in mice eliminates insulin- and AICAR-stimulated glucose transport. *Diabetes* **64**, 746–759 (2015).

21. Sano, H. Insulin-stimulated Phosphorylation of a Rab GTPase-activating Protein Regulates GLUT4 Translocation. *Journal of Biological Chemistry* **278**, 14599–14602 (2003).

22. Treebak, J. T. *et al.* Identification of a novel phosphorylation site on TBC1D4 regulated by AMP-activated protein kinase in skeletal muscle. *American Journal of Physiology-Cell Physiology* (2009) doi:10.1152/ajpcell.00297.2009.

23. Kjøbsted, R. *et al.* Enhanced Muscle Insulin Sensitivity After Contraction/Exercise is Mediated by AMPK. *Diabetes* 1–37 (2016) doi:10.2337/db16-0530.

24. Treebak, J. T. *et al.* Potential role of TBC1D4 in enhanced post-exercise insulin action in human skeletal muscle. *Diabetologia* **52**, 891–900 (2009).

25. Kjøbsted, R. *et al.* TBC1D4-S711 Controls Skeletal Muscle Insulin Sensitization After Exercise and Contraction. *Diabetes* **72**, 857–871 (2023).

26. Skowronek, P. *et al.* Rapid and In-Depth Coverage of the (Phospho-)Proteome With Deep Libraries and Optimal Window Design for dia-PASEF. *Mol Cell Proteomics* **21**, (2022).

27. Humphrey, S. J., Karayel, O., James, D. E. & Mann, M. High-throughput and high-sensitivity phosphoproteomics with the EasyPhos platform. *Nat Protoc* (2018) doi:10.1038/s41596-018-0014-9.

28. Batth, T. S. *et al.* Large-Scale Phosphoproteomics Reveals Shp-2 Phosphatase-Dependent Regulators of Pdgf Receptor Signaling. *Cell Rep* (2018) doi:10.1016/j.celrep.2018.02.038.

29. Hoffman, N. J. *et al.* Global Phosphoproteomic Analysis of Human Skeletal Muscle Reveals a Network of Exercise-Regulated Kinases and AMPK Substrates. *Cell Metab* **22**, 922–935 (2015).

30. Needham, E. J. *et al.* Personalized phosphoproteomics identifies functional signaling. *Nature Biotechnology 2021 40:4* **40**, 576–584 (2021).

31. Blazev, R. *et al.* Phosphoproteomics of three exercise modalities identifies canonical signaling and C18ORF25 as an AMPK substrate regulating skeletal muscle function. *Cell Metab* **34**, 1561-1577.e9 (2022).

32. Deshmukh, A. S. *et al.* Deep Proteomics of Mouse Skeletal Muscle Enables Quantitation of Protein Isoforms, Metabolic Pathways, and Transcription Factors. *Molecular & Cellular Proteomics* **14**, 841–853 (2015).

33. J, F. *et al.* RBM15 suppresses hepatic insulin sensitivity of offspring of Gestational Diabetes Mellitus Mice via m6A-mediated regulation of CLDN4. (2022) doi:10.21203/RS.3.RS-1930111/V1.

34. Johnson, J. L. *et al.* An atlas of substrate specificities for the human serine/threonine kinome. *Nature 2023 613:7945* **613**, 759–766 (2023).

35. Uhlén, M. *et al.* Tissue-based map of the human proteome. *Science (1979)* **347**, (2015).

36. Kim, Y. M. *et al.* SH3BP4 Is a Negative Regulator of Amino Acid-Rag GTPase-mTORC1 Signaling. *Mol Cell* **46**, 833–846 (2012).

37. Møller, A. B. *et al.* Physical exercise increases autophagic signaling through ULK1 in human skeletal muscle. *J Appl Physiol* **118**, 971–979 (2015).

38. O'Neill, B. T. *et al.* Insulin and IGF-1 receptors regulate FoxO-mediated signaling in muscle proteostasis. *J Clin Invest* **126**, 3433 (2016).

39. Baumann, C. A. *et al.* CAP defines a second signalling pathway required for insulin-stimulated glucose transport. *Nature* **407**, 202–207 (2000).

40. Parker, S. S. *et al.* Insulin Induces Microtubule Stabilization and Regulates the Microtubule Plus-end Tracking Protein Network in Adipocytes. *Mol Cell Proteomics* **18**, 1363 (2019).

41. Langlais, P. *et al.* Identification of a Role for CLASP2 in Insulin Action. *J Biol Chem* **287**, 39245 (2012).

42. Osman, A. A. *et al.* Regulation of MAP kinase pathway activity in vivo in human skeletal muscle. *Am J Physiol Endocrinol Metab* **278**, (2000).

43. Krook, A. *et al.* Effects of exercise on mitogen- and stress-activated kinase signal transduction in human skeletal muscle. *Am J Physiol Regul Integr Comp Physiol* **279**, (2000).

44. Karlsson, H. K. R. *et al.* Branched-chain amino acids increase p70S6k phosphorylation in human skeletal muscle after resistance exercise. *Am J Physiol Endocrinol Metab* **287**, (2004).

45. Greiwe, J. S., Kwon, G., McDaniel, M. L. & Semenkovich, C. F. Leucine and insulin activate p70 S6 kinase through different pathways in human skeletal muscle. *Am J Physiol Endocrinol Metab* **281**, (2001).

46. Wang, C. *et al.* Alternative glucose uptake mediated by β-catenin/RSK1 axis under stress stimuli in mammalian cells. *Biochem Pharmacol* **214**, 115645 (2023).

47. Yamaguchi, A., Urano, T., Goi, T. & Feig, L. A. An Eps Homology (EH) Domain Protein That Binds to the Ral-GTPase Target, RalBP1. *Journal of Biological Chemistry* **272**, 31230–31234 (1997).

48. Cullis, D. N., Philip, B., Baleja, J. D. & Feig, L. A. Rab11-FIP2, an Adaptor Protein Connecting Cellular Components Involved in Internalization and Recycling of Epidermal Growth Factor Receptors. *Journal of Biological Chemistry* **277**, 49158–49166 (2002).

49. Kim, S. H. *et al.* Phosphorylation of REPS1 at Ser709 by RSK attenuates the recycling of transferrin receptor. *BMB Rep* **54**, 272 (2021).

50. Dalby, K. N., Morrice, N., Caudwell, F. B., Avruch, J. & Cohen, P. Identification of regulatory phosphorylation sites in mitogen-activated protein kinase (MAPK)-activated protein kinase-1a/p90(rsk) that are inducible by MAPK. *Journal of Biological Chemistry* **273**, 1496–1505 (1998).

51. Aronson, D. *et al.* Exercise stimulates the mitogen-activated protein kinase pathway in human skeletal muscle. *Journal of Clinical Investigation* **99**, 1251 (1997).

52. Wang, S. *et al.* Regulation of cargo exocytosis by a Reps1-Ralbp1-RalA module. *Sci Adv* **9**, (2023).

53. Sollis, E. *et al.* The NHGRI-EBI GWAS Catalog: knowledgebase and deposition resource. *Nucleic Acids Res* **51**, D977–D985 (2023).

54. Machiela, M. J. & Chanock, S. J. LDlink: a web-based application for exploring population-specific haplotype structure and linking correlated alleles of possible functional variants. *Bioinformatics* **31**, 3555–3557 (2015).

55. Myers, T. A., Chanock, S. J. & Machiela, M. J. LDlinkR: An R Package for Rapidly Calculating Linkage Disequilibrium Statistics in Diverse Populations. *Front Genet* **11**, (2020).

56. Altshuler, D. M. *et al.* An integrated map of genetic variation from 1,092 human genomes. *Nature 2012 491:7422* **491**, 56–65 (2012).

57. Ghoussaini, M. *et al.* Open Targets Genetics: systematic identification of trait-associated genes using large-scale genetics and functional genomics. *Nucleic Acids Res* **49**, D1311–D1320 (2021).

58. Foster, L. J. *et al.* A Functional Role for VAP-33 in Insulin-Stimulated GLUT4 Traffic. *Traffic* **1**, 512–521 (2000).

59. Kim, S. H. *et al.* Phosphorylation of REPS1 at Ser709 by RSK attenuates the recycling of transferrin receptor. *BMB Rep* **54**, 272 (2021).

60. Jensen, C. J. *et al.* 90-kDa Ribosomal S6 Kinase Is Phosphorylated and Activated by 3-Phosphoinositide-dependent Protein Kinase-1. *Journal of Biological Chemistry* **274**, 27168–27176 (1999).

61. Lund, S., Holman, G. D., Schmitz, O. & Pedersen, O. Contraction stimulates translocation of glucose transporter GLUT4 in skeletal muscle through a mechanism distinct from that of insulin. *Proc Natl Acad Sci U S A* **92**, 5817 (1995).

62. Jessen, S. *et al.* Muscle hypertrophic effect of inhaled beta2-agonist is associated with augmented insulin-stimulated whole-body glucose disposal in young men. *J Physiol* **600**, 2345–2357 (2022).

63. Jessen, S. *et al.* Hypertrophic effect of inhaled beta2-agonist with and without concurrent exercise training: A randomized controlled trial. *Scand J Med Sci Sports* **28**, 2114–2122 (2018).

64. Andersen, P., Adams, R. P., Sjøgaard, G., Thorboe, A. & Saltin, B. Dynamic knee extension as model for study of isolated exercising muscle in humans. *https://doi.org/10.1152/jappl.1985.59.5.1647* **59**, 1647–1653 (1985).

65. Bergström, J. Percutaneous needle biopsy of skeletal muscle in physiological and clinical research. *Scand J Clin Lab Invest* **35**, 609–616 (1975).

66. Stidsen, J. V. *et al.* Protocol for the specialist supervised individualised multifactorial treatment of new clinically diagnosed type 2 diabetes in general practice (IDA): a prospective controlled multicentre open-label intervention study. *BMJ Open* **7**, (2017).

67. Tarnopolsky, M. A., Pearce, E., Smith, K. & Lach, B. Suction-modified Bergström muscle biopsy technique: experience with 13,500 procedures. *Muscle Nerve* **43**, 716–725 (2011).

68. Meier, F. *et al.* Online Parallel Accumulation-Serial Fragmentation (PASEF) with a Novel Trapped Ion Mobility Mass Spectrometer. *Mol Cell Proteomics* **17**, 2534–2545 (2018).

69. Cox, J. & Mann, M. MaxQuant enables high peptide identification rates, individualized p.p.b.-range mass accuracies and proteome-wide protein quantification. *Nat Biotechnol* **26**, 1367–1372 (2008).

70. Kong, A. T., Leprevost, F. V, Avtonomov, D. M., Mellacheruvu, D. & Nesvizhskii, A. I. MSFragger: Ultrafast and comprehensive peptide identification in mass spectrometry-based proteomics. *Nat Methods* **14**, 513–520 (2017).

71. Tyanova, S. *et al.* The Perseus computational platform for comprehensive analysis of (prote)omics data. *Nature Methods* Preprint at https://doi.org/10.1038/nmeth.3901 (2016).

72. Kim, H. J. *et al.* PhosR enables processing and functional analysis of phosphoproteomic data. *Cell Rep* **34**, 108771 (2021).

73. Ritchie, M. E. *et al.* limma powers differential expression analyses for RNA-sequencing and microarray studies. *Nucleic Acids Res* **43**, e47 (2015).

74. Hornbeck, P. V. *et al.* PhosphoSitePlus, 2014: mutations, PTMs and recalibrations. *Nucleic Acids Res* **43**, D512–D520 (2015).

75. Yu, G., Wang, L. G., Han, Y. & He, Q. Y. clusterProfiler: an R Package for Comparing Biological Themes Among Gene Clusters. *OMICS* **16**, 284 (2012).

76. Jumper, J. *et al.* Highly accurate protein structure prediction with AlphaFold. *Nature 2021 596:7873* **596**, 583–589 (2021).

77. Feizi, A. & Ray, K. otargen: GraphQL-based R package for tidy data accessing and processing from Open Targets Genetics. *Bioinformatics* **39**, (2023).

78. Dalbram, E., Basse, A. L., Zierath, J. R. & Treebak, J. T. Voluntary wheel running in the late dark phase ameliorates diet-induced obesity in mice without altering insulin action. *J Appl Physiol* **126**, 993–1005 (2019).

79. Shi, H. *et al.* Skeletal muscle O-GlcNAc transferase is important for muscle energy homeostasis and whole-body insulin sensitivity. *Mol Metab* **11**, 160–177 (2018).

80. Basse, A. L. *et al.* Nampt controls skeletal muscle development by maintaining Ca2+ homeostasis and mitochondrial integrity. *Volume 53* **53**, (101271).

Acknowledgement

Mass spectrometry analyses were performed by the Proteomics Research Infrastructure (PRI) at the University of Copenhagen (UCPH), supported by the Novo Nordisk Foundation (NNF) (grant agreement number NNF19SA0059305). This work is supported by an unconditional donation from the Novo Nordisk Foundation (NNF) to NNF Center for Basic Metabolic Research (http://www.cbmr.ku.dk (1 July 2018) (Grant number NNF18CC0034900). The T2D study was supported by grants from the Region of Southern Denmark, the Novo Nordisk Foundation (Grant number NNF15OC0015986), and from The Sawmill Owner Jeppe Juhl and wife Ovita Juhl Memorial Foundation. Mario Garcia Ureña and Tuomas O. Kilpeläinen were supported by the NNF grant number NNF22OC0074128. We want to thank Professor Amira Klip for kindly donating the L6-myc-GLUT4 cells used in the manuscript.

Author information

Author affiliations

Novo Nordisk Foundation Center for Basic Metabolic Research, Faculty of Health and Medical Sciences, University of Copenhagen, Copenhagen, Denmark

Jeppe Kjærgaard Larsen, Cecilie B. Lindqvist, Mario García-Ureña, Amy M. Ehrlich, Farina Schlabs, Júlia Prats Quesada, Johann H. Schmalbruch, Lewin Small, Alba Gonzalez-Franquesa, Tuomas O. Kilpeläinen, Jonas T. Treebak, Atul S. Deshmukh

The August Krogh Section for Human Physiology, Department of Nutrition, Exercise and Sports, University of Copenhagen, Copenhagen, Denmark

Søren Jessen, Martin Thomassen, Anders Krogh Lemminger, Kasper Eibye, Jens Bangsbo, Morten Hostrup

Steno Diabetes Center Odense, Odense University Hospital, Odense C, Denmark

Jacob V. Stidsen, Kurt Højlund

Department of Clinical Research, University of Southern Denmark, Odense C, Denmark

Kurt Højlund

Contributions

Conceptualization, MH, JKL and ASD; Human clinical studies, JVS, KH, MH, JB, KE, SJ, AKL, MT; Investigation, JKL, CBL, MGU, AME, FS, JP, JHS, LS, MT, AGF, TOK, JTT; Writing – Original

Draft, JKL and ASD; Writing – Review & Editing, All; Funding Acquisition, ASD, MH and KH; Resources, ASD and MH; Supervision, ASD and MH.

Ethics declarations

Competing interests

The authors declare no competing interests.

Figure Legends

Figure 1. Phosphoproteomic Signature of Insulin and Exercise Signaling in Human Skeletal Muscle. Study design – Eight healthy men underwent, in randomized order, an acute bout of high intensity cycling exercise (study day 1) and a hyperinsulinemic-euglycemic clamp (study day 2). Skeletal muscle biopsies were obtained pre and immediately post each intervention (A). Glycogen content (B) and leg glucose balance during clamp (C). Western blot confirmation of insulin and exercise-induced signaling (D). Phosphoproteomics workflow with 2x TMT 11-plex labelling, phosphopeptide enrichment and LC-MS/MS analysis (E). Principal component analysis of insulin and exercise signaling responses (F-G). Volcano plots of insulin and exercise signaling (x-axis = logFC, y-axis = -log10 (*P* value)). A linear model (Limma) was used to test for difference in phosphosite abundance between conditions with a false-discovery rate set to 5% (H-I). $P < 0.01$ = **.

Figure 2. Shared and Distinct Features of Insulin and Exercise Signaling. Predicted insulin- and exercise-activated kinases from the kinase library (A-B). Two-sided Fisher's exact test of phosphosite functionality based on the PhosphoSitePlus database (C). Heatmap of individual fold-change response of significant phosphosites to exercise and insulin stimulation across the five subjects (D). Selected phosphosites regulated in opposite or the same direction (E). Alpha-fold predicted structure of CLASP2 with highlighted serine residues phosphorylated or dephosphorylated by both insulin and exercise (F). Sequence window of phosphosites upregulated by insulin and exercise. A Two-sided Fisher's exact test was used to test for residue overrepresentation (G). Kinase enrichment analysis of phosphosites upregulated by both insulin and exercise (H). Individual fold-changes of p-REPS1 S709 in response to insulin and exercise (I). $P < 0.05$ = *, $P < 0.01$ = **, $P < 0.001$ = ***.

Figure 3. The Insulin and Exercise-responsive Protein, REPS1, is a Critical Regulator of Skeletal Muscle Glucose Uptake. Highly conserved REPS1 sequence window around the serine 709 site (A). Western blot validation of REPS1 phosphorylation in human skeletal muscle before (basal) and after (insulin) a two-hour hyperinsulinemic euglycemic clamp (B) and at rest and after 10 minutes high intensity cycling exercise (C). Pearson's correlation analysis of steady-state leg glucose uptake and delta (Post-Pre clamp) REPS1 S709 phosphorylation (D). In vivo ^{3}H-2-deoxy-glucose uptake during rest or *in situ* contractions of tibialis anterior (TA) muscle with saline or 15 mU insulin stimulation (E). Pearson's correlation analysis of insulin-stimulated glucose uptake into TA muscle and REPS1 S709 phosphorylation (F). Representative western blot from *in situ* contraction experiment (H). Western blot validation of SiRNA-mediated

knockdown of *Reps1* in C2C12 myotubes (I). Insulin-stimulated ^{3}H-2-deoxy-glucose uptake in C2C12 myotubes transfected with control or *Reps1* siRNA (J). Data in B and C were analyzed with a two-sided paired sample t-test (n = 8). Data in E and F were analyzed by a two-way ANOVA with repeated measures and Sidak multiple comparison test (n = 7-10). Data in I were analyzed by a two-sided two sample t-test. Data in J were analyzed by two-away-ANOVA with Tukey's multiple comparisons test (n=6) (J). $P < 0.05$ = *, $P < 0.01$ = **, $P < 0.001$ = ***.

Figure 4. RSK is an Upstream Kinase of REPS1 S709 and is Associated with Vesicle-Sorting Proteins in Skeletal Muscle. Insulin-stimulated (100 nM, 10 minutes) glucose uptake in C2C12 myotubes preincubated (20 minutes) with DMSO or 10 μM of the RSK inhibitor, BI-D1870 (A). Quantified western blot analysis of signaling as in A (B). Representative western blot analysis for signaling in B (C). Insulin-stimulated (100nM, 10 minutes) GLUT4-tranlocation in L6 myotubes preincubated (20 minutes) with DMSO or 10 μM BI-D1870 (D). Basal and insulin-stimulated (300μIU/mL, 30 minutes) glucose uptake in *ex vivo* incubated mouse soleus muscle preincubated (60 minutes) with DMSO or 10 μM BI-D1870 (E). Quantified western blot analysis of signaling as in E (F-G). Representative images of western blot analysis for signaling in *ex vivo* incubated muscles (H). Flag-Pull-down of C2C12 myotubes transduced with either FLAG-*Reps1* vs FLAG-CTR (I). Differentially enriched proteins highlighted in blue (two-sample t-test, FDR < 5%). Illustration of signaling pathways affected and the proposed role of REPS1 in vesicle trafficking (J). Illustration made in Biorender. $P < 0.001$ = ***. Data in A and B were analyzed by two-away-ANOVA with Tukey's multiple comparisons test.

Figure 5. Insulin-induced REPS1 S709 phosphorylation *in vivo* is Impaired in Multiple Models of Insulin Resistance. Sixteen C57BL6 male mice (7 weeks old) were fed a low-fat diet (LFD; n = 8) or high-fat-diet (HFD; n = 8) for 16 weeks. At day of termination, mice were injected with either saline or 1U/kg insulin and tissues were collected after 15 minutes (n = 4) (A). Body weight of mice after 16-weeks of diet intervention and blood glucose (mM) delta (post-pre) values in response to saline/insulin injection (B). Corresponding western blot analysis of insulin signaling in epidydimal white adipose tissue (eWAT), quadriceps muscle and liver tissue from same animals (C). BMI and glucose-infusion rate (GIR) in response to a hyperinsulinemic euglycemic clamp (4 hrs) of 10 normal glucose tolerant (NGT) and 10 patients with T2D (D). Quantified Western blot of REPS1 S709 phosphorylation pre and post insulin stimulation (E). Association of GIR and delta REPS1 S709 phosphorylation in skeletal muscle (F). Data in B-C were analyzed by a two-way ANOVA and Tukey's multiple comparisons test. Data in E were analyzed by a two-way ANOVA with repeated measures and Sidak multiple comparisons test. Data in F were analyzed by

ANCOVA analysis followed by individual Pearson correlation (F). $P < 0.05$ = *, $P < 0.01$ = **, $P < 0.001$ = ***.

Figure 6. REPS1 Variants' Associations with Complex Traits, mRNA Expression, and Splicing. Lower segment: Representation of the phenotypes associated with *REPS1* variants using data from NHGRI-EBI GWAS Catalog and Open Target Genetics. In total we identified 6 independent signals ($r^2 < 0.1$) in the *REPS1* region: 4 were located in *REPS1* introns and 2 in an intergenic region between *REPS1* and *ABRACL*. Each signal is represented by their lead variant. Upper segment: Representation of tissues and cell types with significant changes in *REPS1* expression (eQTL) or alternative splicing (sQTL) as reported in Open Target Genetics. We report all tissues and cell types with significant eQTL or sQTL associations for any of the 6 independent *REPS1* lead variants. See Supplementary Tables 2A-C for more information on the associations for each lead variant.

Supplemental Figure Legends

Figure S1. Phosphoproteomic Signature of Insulin and Exercise Signaling in Human Skeletal Muscle. Levels of plasma epinephrine (A), norepinephrine (B) in response to the acute bout of exercise and during the insulin clamp (C-D). Levels of plasma insulin during the insulin clamp (E) and in response to the acute bout of exercise (F). Quantified western blot analysis of p-mTOR S2448 (A), p-AKT S473 (B), p-AMPK T172 (C) and p-ACC S221 (D) in human skeletal muscle pre/post an hyperinsulinemic euglycemic clamp (2hr) and pre/post 10 minutes of high intensity cycling exercise. Paired-Samples t-test was used to analyze mean differences within each experiment. $P < 0.05$ = *, $P < 0.01$ = **, $P < 0.001$ = ***.

Figure S2 - Shared and Distinct Features of Insulin and Exercise Signaling. Gene Ontology (GO) overrepresentation test was used to assess enrichment for Biological Processes within phosphoproteins being phosphorylated (A) or dephosphorylated (B) by both insulin/exercise. The whole phosphoprotein proteome was used as background. Only BP-terms with a Benjamini Hochberg-adjusted *P* value below 5% is shown. Representation of individual fold changes for CLASP2 S327 (C), CLASP1 S600 (D) and CLASP1 S559 (E) in response to insulin stimulation and an acute bout of exercise by LC-MS/MS.

Figure S3. The Insulin and Exercise-responsive Protein, REPS1, is a Critical Regulator of Skeletal Muscle Glucose Uptake. Pearson's correlation analysis of leg steady-state glucose

uptake with delta (Post-Pre) p-AKT S473 (A) and p-mTOR S2448 levels (B) measured by western blot. Pearson's correlation analysis of delta (Contracted-Rested) glucose uptake and REPS1 S709 phosphorylation (C).

Figure S4. RSK is an Upstream Kinase of REPS1 S709 and is Associated with Vesicle-Sorting Proteins in Skeletal Muscle. Quantified western blot of C2C12 myotubes pretreated with DMSO or 10 μM BI-D1870 for 20 minutes minutes before 10 minutes of 100 nM insulin stimulation (A). Quantified western blot of C2C12 myotubes pretreated with DMSO, Rapamycin (100 nM) or PF-4708671 (10 μM) for 20 minutes before 10 minutes of 100 nM insulin stimulation (B-C). Representative western blot images for the result presented in B-C (D). Quantified western blot of C2C12 myotubes pretreated with 10 μM MP-7 for 20 minutes followed by 10 minutes of 100 nM insulin stimulation (E-F). Representative western blot images for the results presented in E-F (G). Quantified western blot of C2C12 myotubes pretreated DMSO or 10 μM U0126 for 20 minutes before 10 minutes of 100 nM insulin stimulation (H-I). Representative western blot images for the results presented in H-I (J). Endogenous IP of REPS1 vs IgG control IP (K). Differentially enriched proteins highlighted in dark blue (two-sample t-test, FDR < 5%). GO-enrichment analysis of significant interactors found in both pull-down and endogenous IP experiments (L). Whole interactome was used as background. Table showing significant interactors (< 5% FDR) in Flag- and endogenous-IP experiments with log2 fold changes (M).

Figure S5. Insulin-induced REPS1 S709 phosphorylation *in vivo* is Impaired in Multiple Models of Insulin Resistance. Association of insulin-lowering (delta 15-0 min) blood glucose (BG) and REPS1 S709 phosphorylation in insulin-stimulated quadriceps skeletal muscle from LFD and HFD fed mice (A).

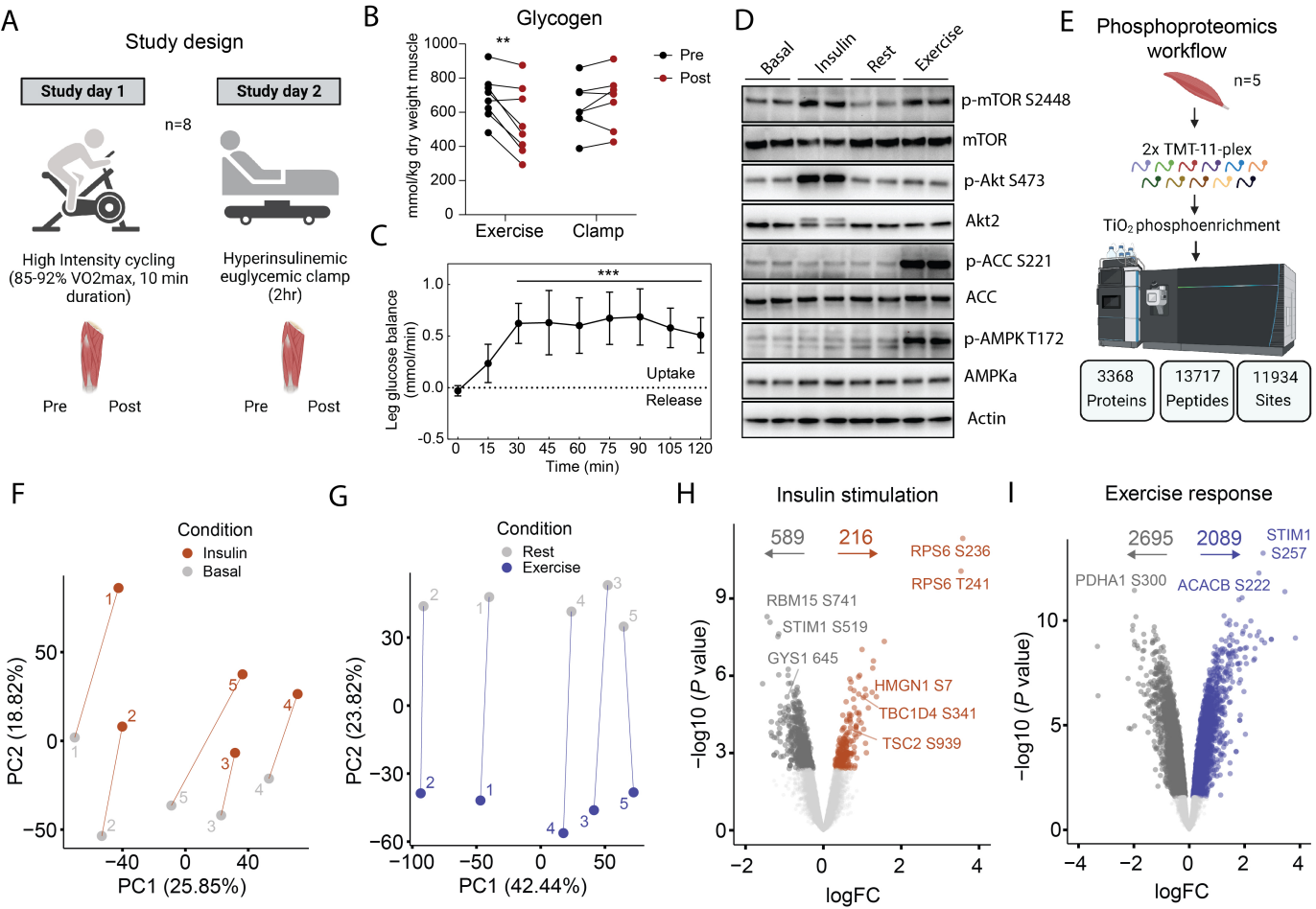
A
Study design
Study day 1
Study day 2
n=8
High Intensity cycling (85-92% VO2max, 10 min duration)
Hyperinsulinemic euglycemic clamp (2hr)
Pre
Post
Pre
Post
B
Glycogen
mmol/kg dry weight muscle
1000
800
600
400
200
0
**
Pre
Post
Exercise
Clamp
C
Leg glucose balance (mmol/min)
1.0
0.5
0.0
-0.5
***
Uptake
Release
0
15
30
45
60
75
90
105
120
Time (min)
D
Basal
Insulin
Rest
Exercise
p-mTOR S2448
mTOR
p-Akt S473
Akt2
p-ACC S221
ACC
p-AMPK T172
AMPKa
Actin
E
Phosphoproteomics workflow
n=5
2x TMT-11-plex
TiO2 phosphoenrichment
3368 Proteins
13717 Peptides
11934 Sites
F
Condition
Insulin
Basal
PC2 (18.82%)
PC1 (25.85%)
50
0
−50
−40
0
40
G
Condition
Rest
Exercise
PC2 (23.82%)
PC1 (42.44%)
30
0
−30
−60
−100
−50
0
50
H
Insulin stimulation
589
216
RPS6 S236
RPS6 T241
RBM15 S741
STIM1 S519
GYS1 645
HMGN1 S7
TBC1D4 S341
TSC2 S939
−log10 (P value)
logFC
9
6
3
0
−2
0
2
4
I
Exercise response
2695
2089
STIM1 S257
PDHA1 S300
ACACB S222
−log10 (P value)
logFC
10
5
0
−4
−2
0
2
4

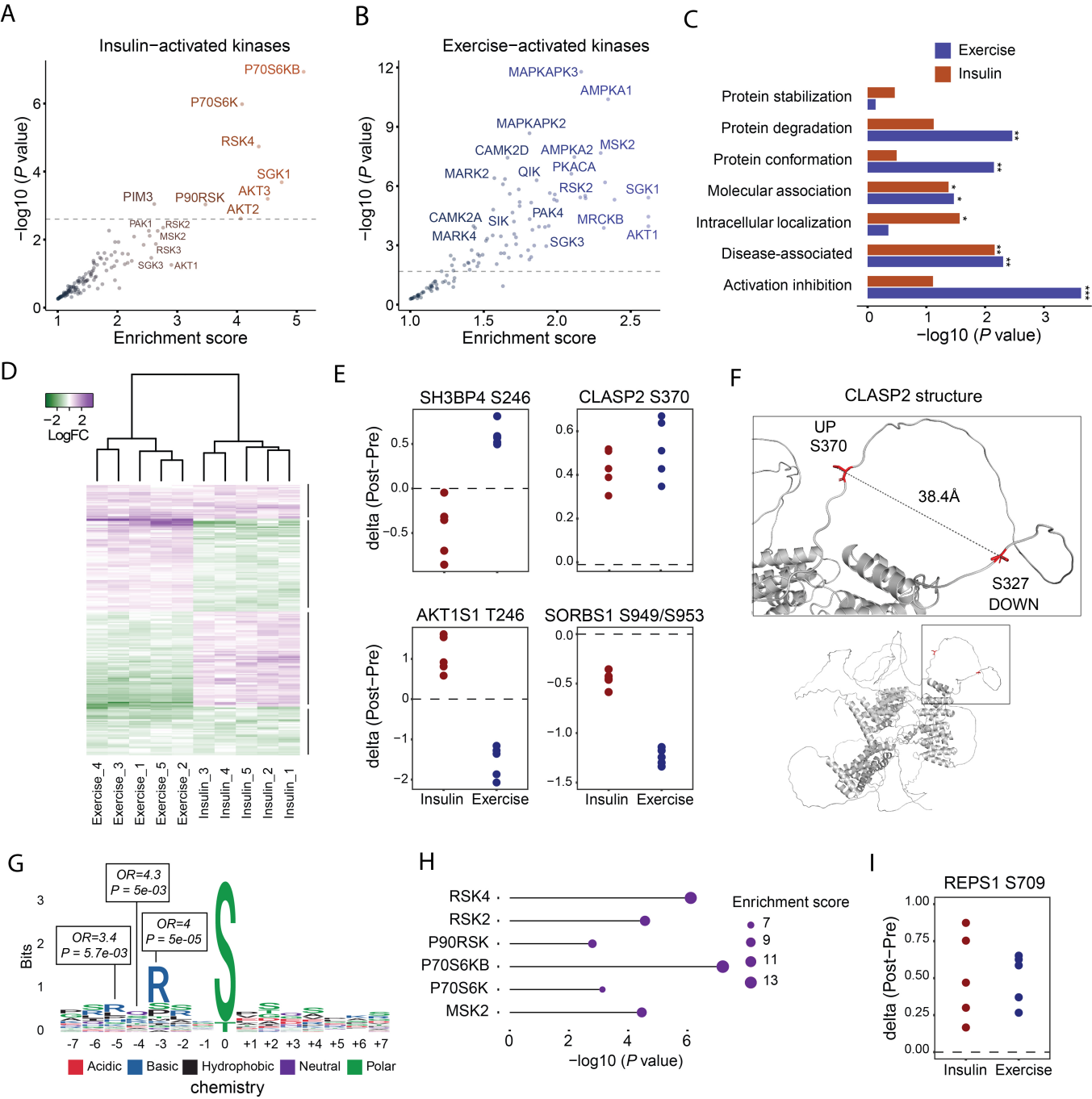
A
Insulin−activated kinases
P70S6KB
P70S6K
RSK4
SGK1
AKT3
AKT2
PIM3
P90RSK
PAK1
RSK2
MSK2
RSK3
SGK3
AKT1
−log10 (P value)
Enrichment score
B
Exercise−activated kinases
MAPKAPK3
AMPKA1
MAPKAPK2
CAMK2D
AMPKA2
MSK2
MARK2
QIK
PKACA
RSK2
SGK1
CAMK2A
SIK
PAK4
MRCKB
MARK4
SGK3
AKT1
−log10 (P value)
Enrichment score
C
Exercise
Insulin
Protein stabilization
Protein degradation
Protein conformation
Molecular association
Intracellular localization
Disease-associated
Activation inhibition
−log10 (P value)
D
LogFC
Exercise_4
Exercise_3
Exercise_1
Exercise_5
Exercise_2
Insulin_3
Insulin_4
Insulin_5
Insulin_2
Insulin_1
E
SH3BP4 S246
CLASP2 S370
AKT1S1 T246
SORBS1 S949/S953
delta (Post−Pre)
Insulin
Exercise
F
CLASP2 structure
UP
S370
38.4Å
S327
DOWN
G
OR=4.3
P = 5e-03
OR=3.4
P = 5.7e-03
OR=4
P = 5e-05
Bits
Acidic
Basic
Hydrophobic
Neutral
Polar
chemistry
H
RSK4
RSK2
P90RSK
P70S6KB
P70S6K
MSK2
Enrichment score
−log10 (P value)
I
REPS1 S709
delta (Post−Pre)
Insulin
Exercise

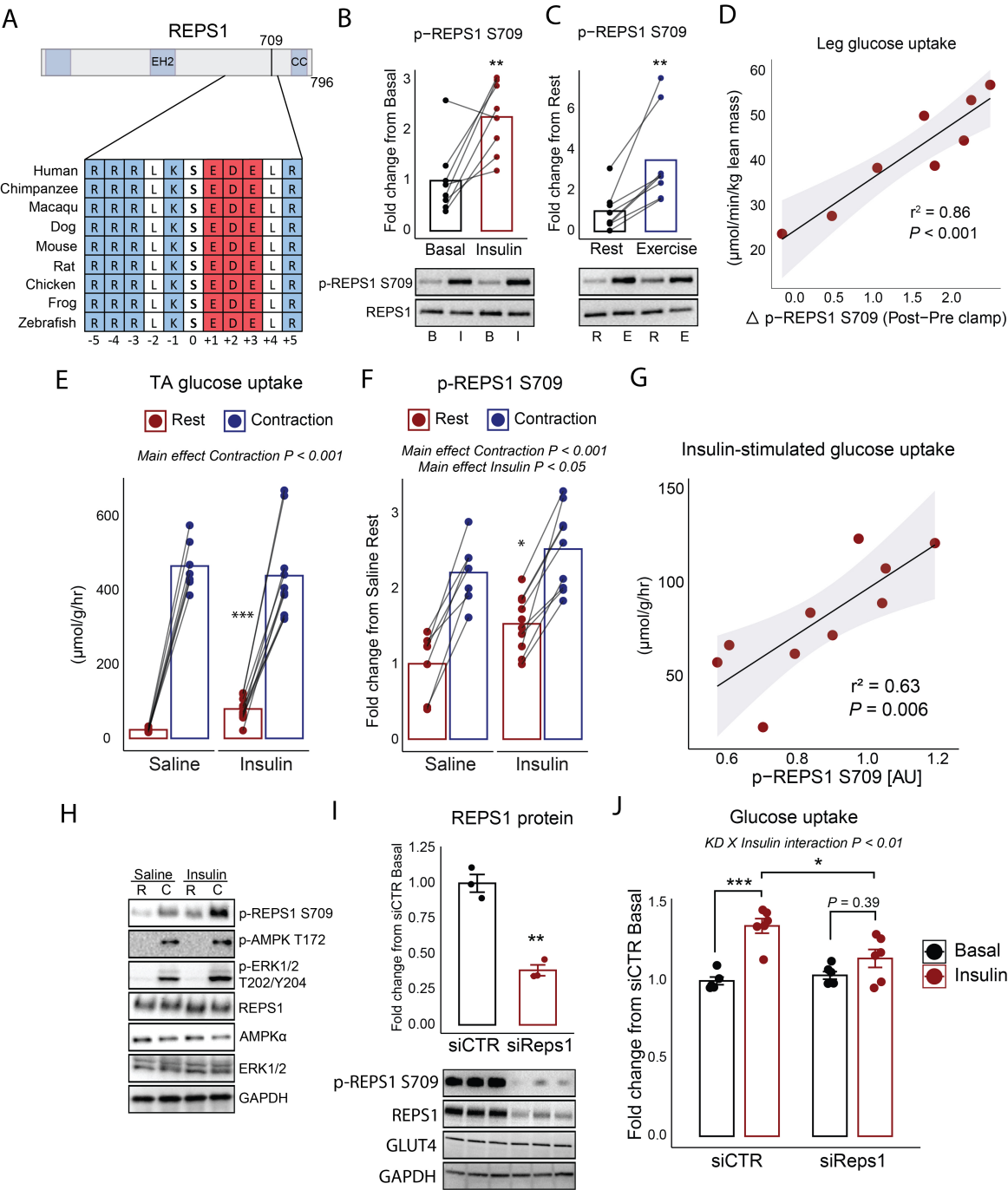
A
REPS1
709
EH2
CC
796
Human R R R L K S E D E L R
Chimpanzee R R R L K S E D E L R
Macaqu R R R L K S E D E L R
Dog R R R L K S E D E L R
Mouse R R R L K S E D E L R
Rat R R R L K S E D E L R
Chicken R R R L K S E D E L R
Frog R R R L K S E D E L R
Zebrafish R R R L K S E D E L R
-5 -4 -3 -2 -1 0 +1 +2 +3 +4 +5
B
p-REPS1 S709
Fold change from Basal
Basal Insulin
p-REPS1 S709
REPS1
B I B I
C
p-REPS1 S709
Fold change from Rest
Rest Exercise
R E R E
D
Leg glucose uptake
(µmol/min/kg lean mass)
r² = 0.86
P < 0.001
Δ p-REPS1 S709 (Post-Pre clamp)
E
TA glucose uptake
Rest
Contraction
Main effect Contraction P < 0.001
(µmol/g/hr)
Saline Insulin
F
p-REPS1 S709
Rest
Contraction
Main effect Contraction P < 0.001
Main effect Insulin P < 0.05
Fold change from Saline Rest
Saline Insulin
G
Insulin-stimulated glucose uptake
(µmol/g/hr)
r² = 0.63
P = 0.006
p-REPS1 S709 [AU]
H
Saline Insulin
R C R C
p-REPS1 S709
p-AMPK T172
p-ERK1/2 T202/Y204
REPS1
AMPKα
ERK1/2
GAPDH
I
REPS1 protein
Fold change from siCTR Basal
siCTR siReps1
p-REPS1 S709
REPS1
GLUT4
GAPDH
J
Glucose uptake
KD X Insulin interaction P < 0.01
P = 0.39
Fold change from siCTR Basal
Basal
Insulin
siCTR siReps1

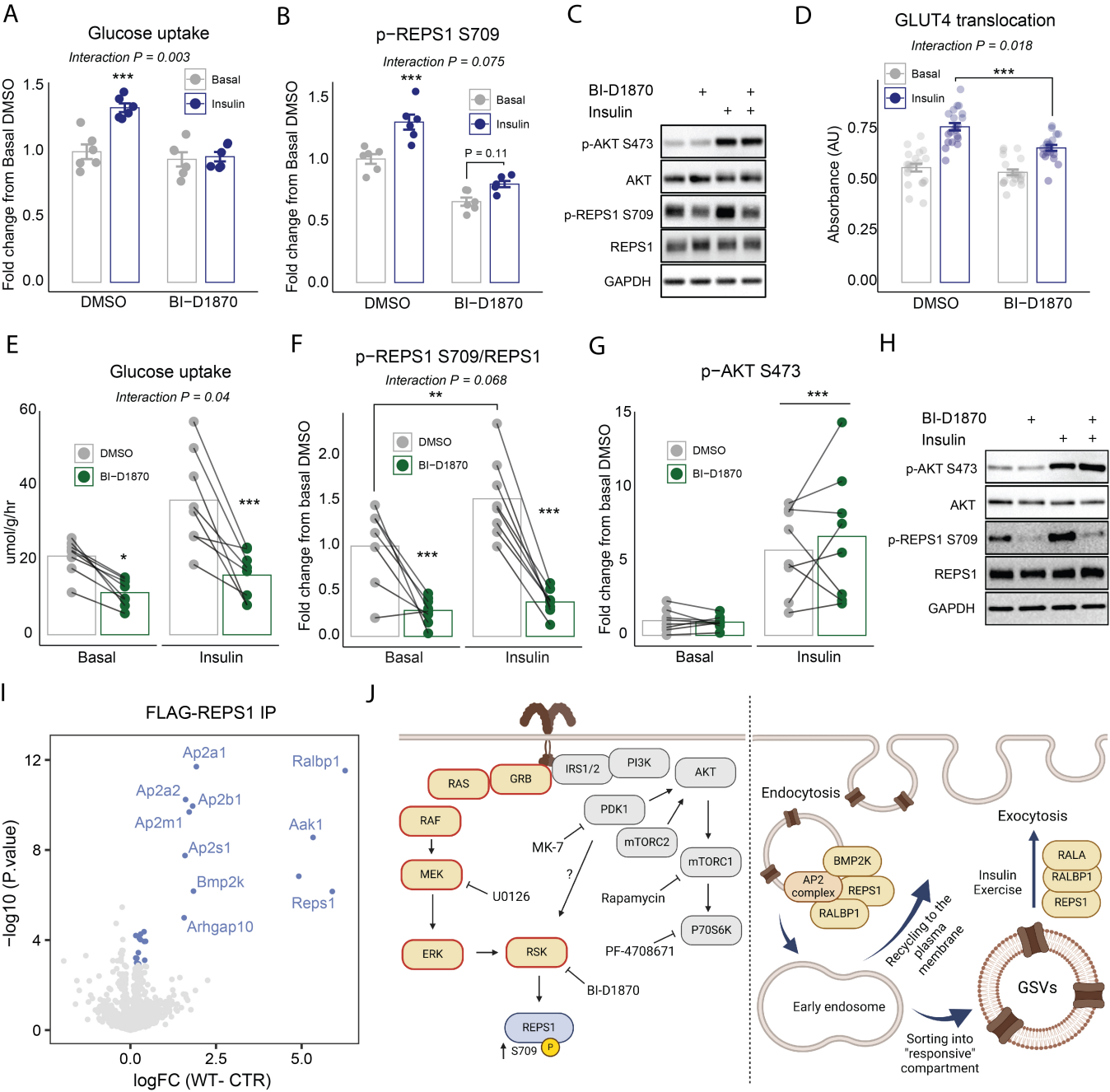
A
Glucose uptake
Interaction P = 0.003
Basal
Insulin
Fold change from Basal DMSO
DMSO
BI−D1870
B
p−REPS1 S709
Interaction P = 0.075
P = 0.11
C
BI-D1870
Insulin
p-AKT S473
AKT
p-REPS1 S709
REPS1
GAPDH
D
GLUT4 translocation
Interaction P = 0.018
Absorbance (AU)
E
Glucose uptake
Interaction P = 0.04
umol/g/hr
F
p−REPS1 S709/REPS1
Interaction P = 0.068
Fold change from basal DMSO
G
p−AKT S473
H
I
FLAG-REPS1 IP
Ap2a1
Ralbp1
Ap2a2
Ap2b1
Ap2m1
Aak1
Ap2s1
Bmp2k
Reps1
Arhgap10
−log10 (P.value)
logFC (WT- CTR)
J
RAS
GRB
IRS1/2
PI3K
AKT
RAF
PDK1
mTORC2
MK-7
MEK
U0126
mTORC1
Rapamycin
P70S6K
PF-4708671
ERK
RSK
BI-D1870
REPS1
S709
P
Endocytosis
Exocytosis
BMP2K
AP2 complex
REPS1
RALBP1
Insulin Exercise
RALA
RALBP1
REPS1
Recycling to the plasma membrane
Early endosome
GSVs
Sorting into "responsive" compartment

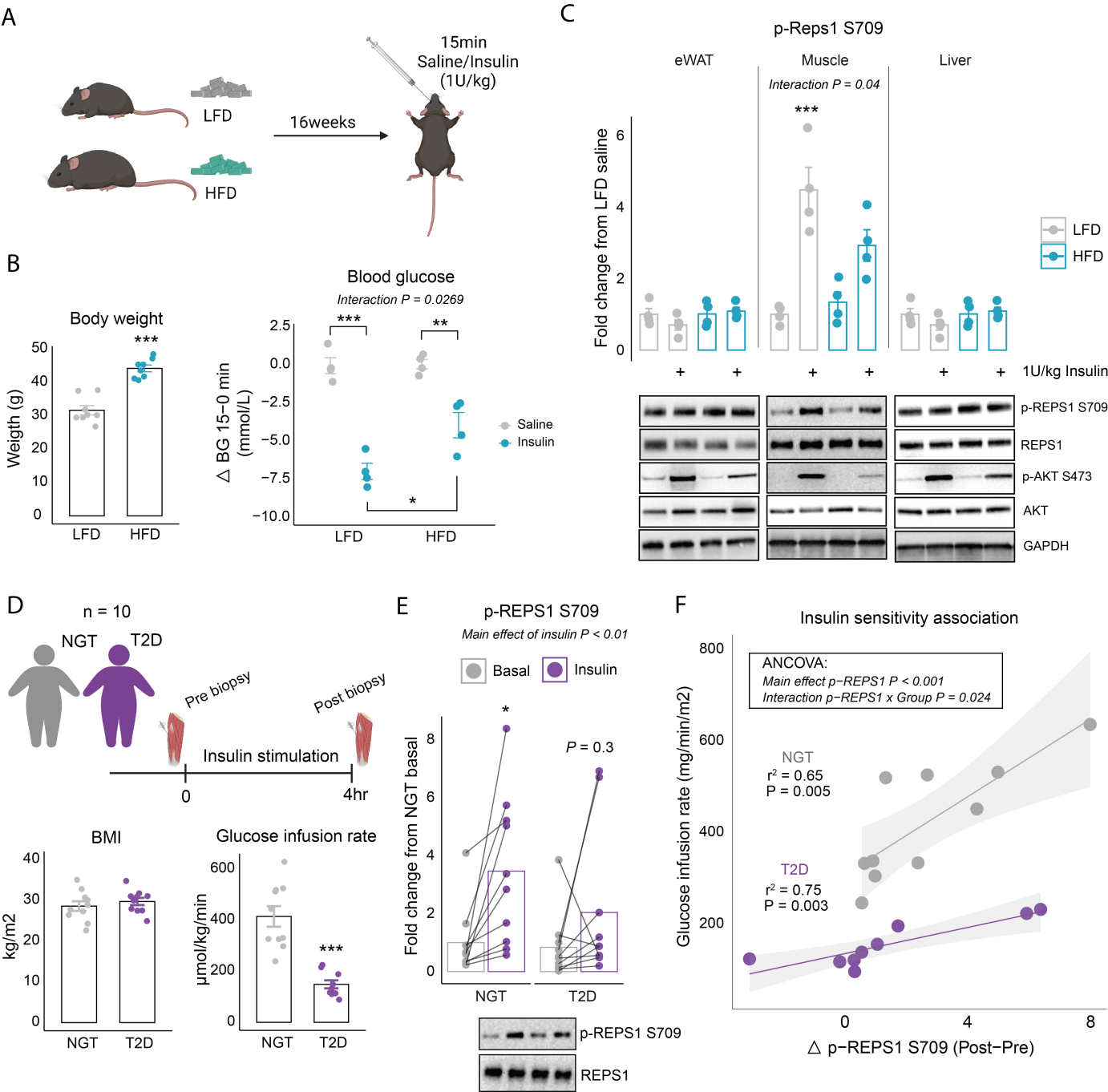
A
LFD
HFD
16weeks
15min
Saline/Insulin
(1U/kg)
B
Body weight
***
Weigth (g)
50
40
30
20
10
0
LFD
HFD
Blood glucose
Interaction P = 0.0269
***
**
*
△ BG 15−0 min
(mmol/L)
2.5
0.0
−2.5
−5.0
−7.5
−10.0
Saline
Insulin
LFD
HFD
C
p-Reps1 S709
eWAT
Muscle
Liver
Interaction P = 0.04
***
Fold change from LFD saline
6
4
2
0
LFD
HFD
1U/kg Insulin
p-REPS1 S709
REPS1
p-AKT S473
AKT
GAPDH
D
n = 10
NGT
T2D
Pre biopsy
Post biopsy
Insulin stimulation
0
4hr
BMI
kg/m2
40
30
20
10
0
NGT
T2D
Glucose infusion rate
μmol/kg/min
600
400
200
0
***
NGT
T2D
E
p-REPS1 S709
Main effect of insulin P < 0.01
Basal
Insulin
*
P = 0.3
Fold change from NGT basal
8
6
4
2
0
NGT
T2D
p-REPS1 S709
REPS1
F
Insulin sensitivity association
ANCOVA:
Main effect p−REPS1 P < 0.001
Interaction p−REPS1 x Group P = 0.024
NGT
r2 = 0.65
P = 0.005
T2D
r2 = 0.75
P = 0.003
Glucose infusion rate (mg/min/m2)
800
600
400
200
0
4
8
△ p−REPS1 S709 (Post−Pre)

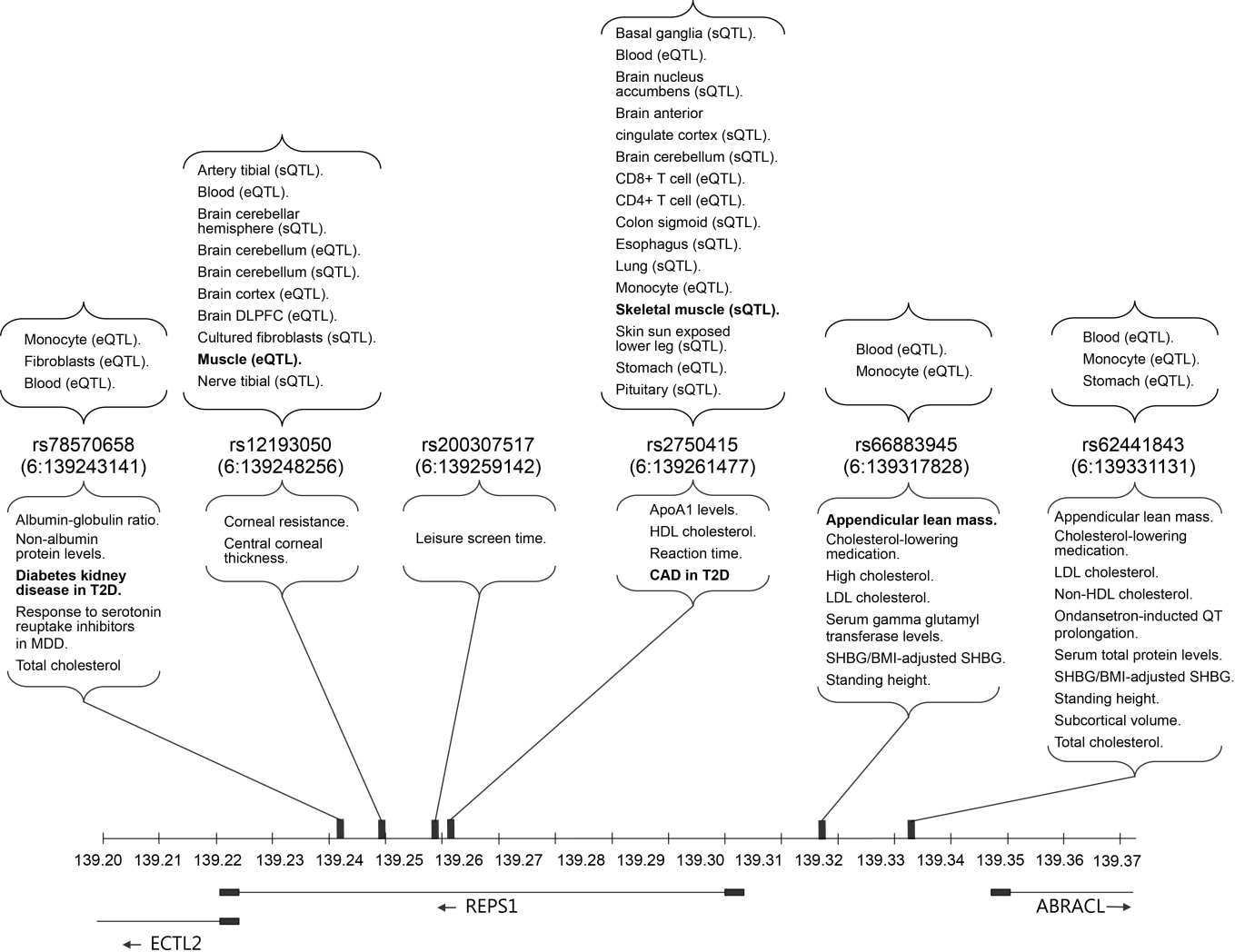
Basal ganglia (sQTL).
Blood (eQTL).
Brain nucleus accumbens (sQTL).
Brain anterior cingulate cortex (sQTL).
Brain cerebellum (sQTL).
CD8+ T cell (eQTL).
CD4+ T cell (eQTL).
Colon sigmoid (sQTL).
Esophagus (sQTL).
Lung (sQTL).
Monocyte (eQTL).
Skeletal muscle (sQTL).
Skin sun exposed lower leg (sQTL).
Stomach (eQTL).
Pituitary (sQTL).
Artery tibial (sQTL).
Blood (eQTL).
Brain cerebellar hemisphere (sQTL).
Brain cerebellum (eQTL).
Brain cerebellum (sQTL).
Brain cortex (eQTL).
Brain DLPFC (eQTL).
Cultured fibroblasts (sQTL).
Muscle (eQTL).
Nerve tibial (sQTL).
Monocyte (eQTL).
Fibroblasts (eQTL).
Blood (eQTL).
Blood (eQTL).
Monocyte (eQTL).
Blood (eQTL).
Monocyte (eQTL).
Stomach (eQTL).
rs78570658 (6:139243141)
rs12193050 (6:139248256)
rs200307517 (6:139259142)
rs2750415 (6:139261477)
rs66883945 (6:139317828)
rs62441843 (6:139331131)
Albumin-globulin ratio.
Non-albumin protein levels.
Diabetes kidney disease in T2D.
Response to serotonin reuptake inhibitors in MDD.
Total cholesterol
Corneal resistance.
Central corneal thickness.
Leisure screen time.
ApoA1 levels.
HDL cholesterol.
Reaction time.
CAD in T2D
Appendicular lean mass.
Cholesterol-lowering medication.
High cholesterol.
LDL cholesterol.
Serum gamma glutamyl transferase levels.
SHBG/BMI-adjusted SHBG.
Standing height.
Appendicular lean mass.
Cholesterol-lowering medication.
LDL cholesterol.
Non-HDL cholesterol.
Ondansetron-inducted QT prolongation.
Serum total protein levels.
SHBG/BMI-adjusted SHBG.
Standing height.
Subcortical volume.
Total cholesterol.
139.20 139.21 139.22 139.23 139.24 139.25 139.26 139.27 139.28 139.29 139.30 139.31 139.32 139.33 139.34 139.35 139.36 139.37
REPS1
ABRACL
ECTL2

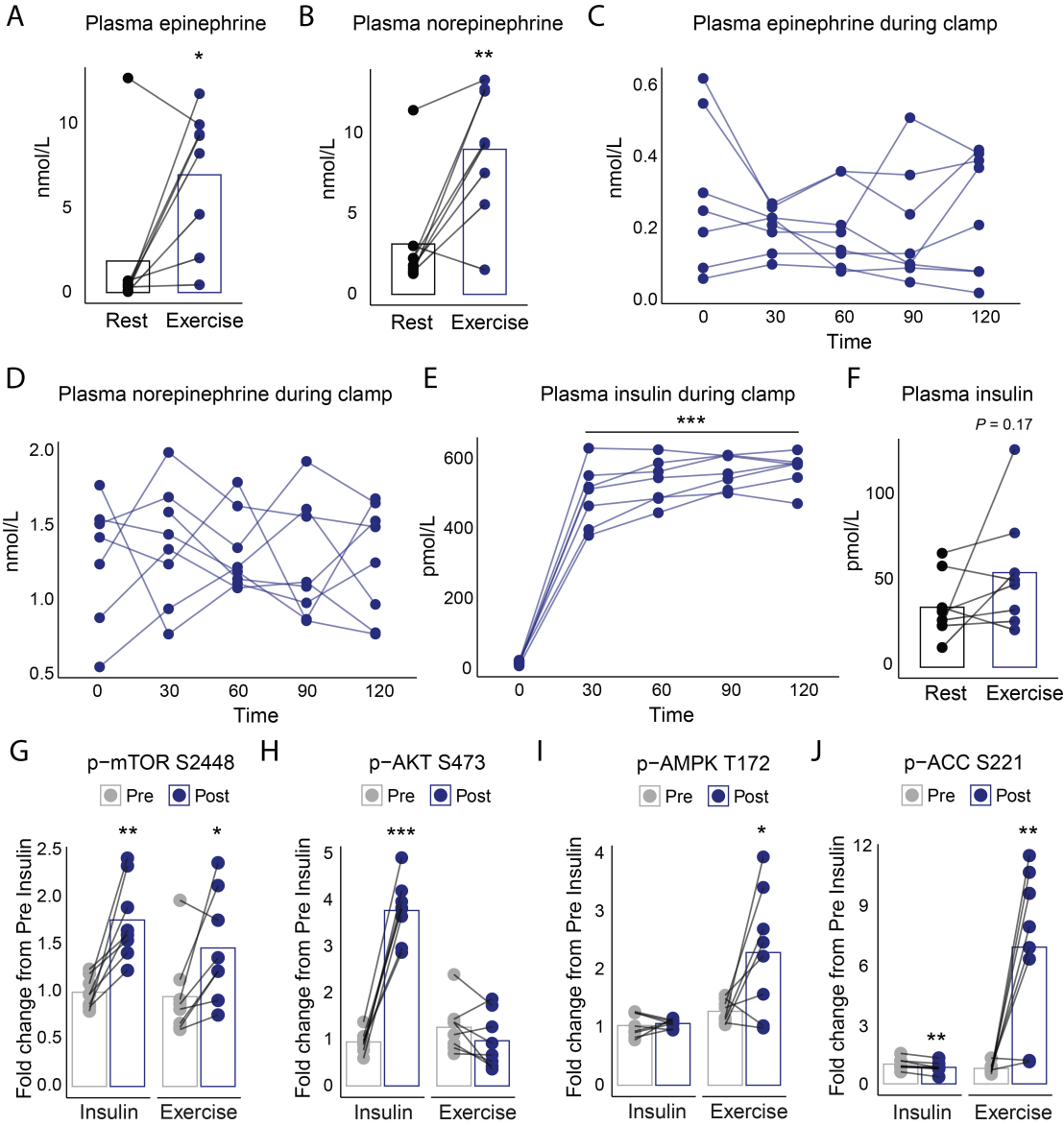
A
Plasma epinephrine
nmol/L
Rest
Exercise
B
Plasma norepinephrine
C
Plasma epinephrine during clamp
Time
D
Plasma norepinephrine during clamp
E
Plasma insulin during clamp
pmol/L
F
Plasma insulin
P = 0.17
G
p−mTOR S2448
Pre
Post
Fold change from Pre Insulin
Insulin
Exercise
H
p−AKT S473
I
p−AMPK T172
J
p−ACC S221

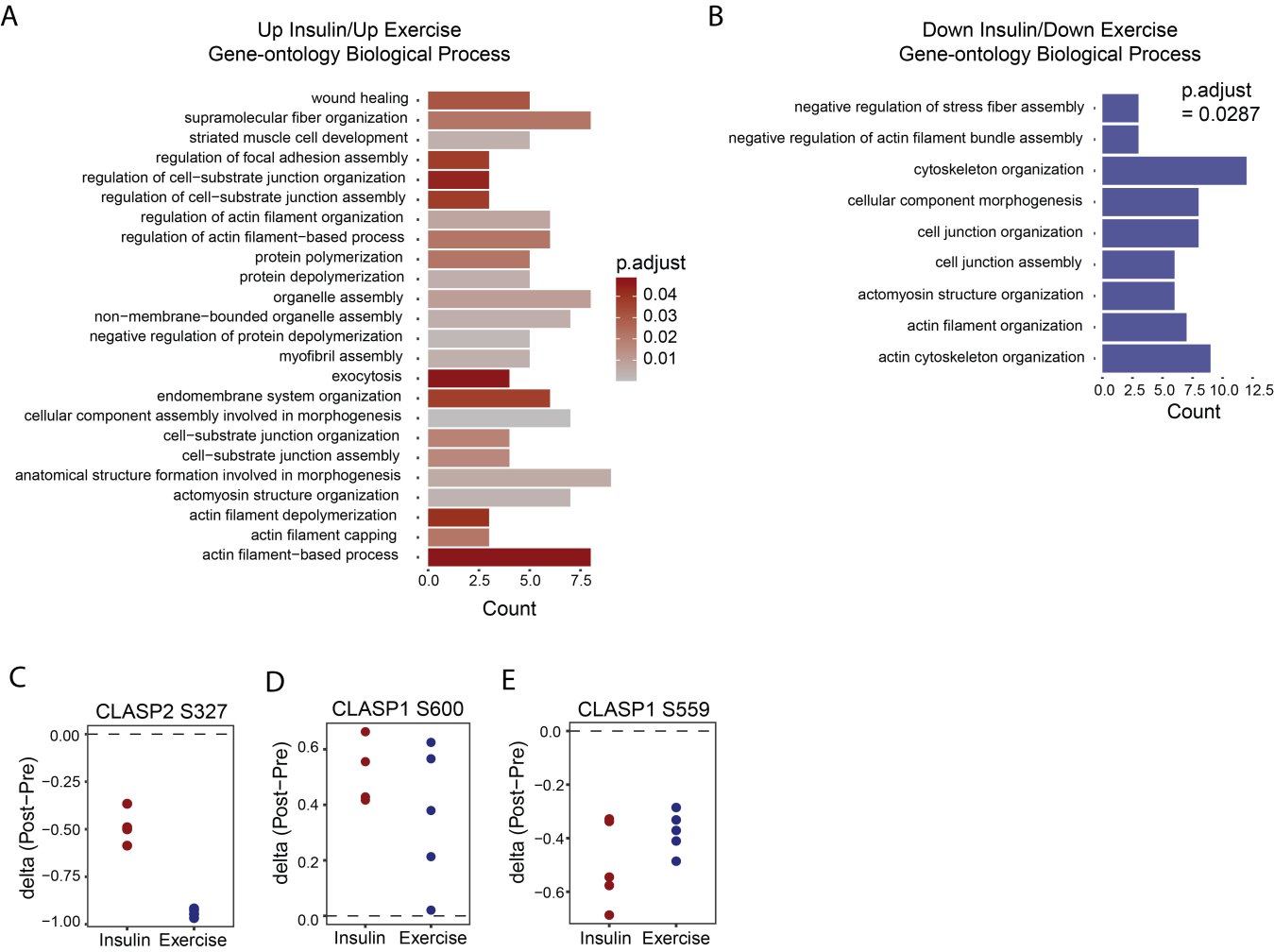
A
Up Insulin/Up Exercise
Gene-ontology Biological Process
wound healing
supramolecular fiber organization
striated muscle cell development
regulation of focal adhesion assembly
regulation of cell−substrate junction organization
regulation of cell−substrate junction assembly
regulation of actin filament organization
regulation of actin filament−based process
protein polymerization
protein depolymerization
organelle assembly
non−membrane−bounded organelle assembly
negative regulation of protein depolymerization
myofibril assembly
exocytosis
endomembrane system organization
cellular component assembly involved in morphogenesis
cell−substrate junction organization
cell−substrate junction assembly
anatomical structure formation involved in morphogenesis
actomyosin structure organization
actin filament depolymerization
actin filament capping
actin filament−based process
0.0
2.5
5.0
7.5
Count
p.adjust
0.04
0.03
0.02
0.01
B
Down Insulin/Down Exercise
Gene-ontology Biological Process
negative regulation of stress fiber assembly
negative regulation of actin filament bundle assembly
cytoskeleton organization
cellular component morphogenesis
cell junction organization
cell junction assembly
actomyosin structure organization
actin filament organization
actin cytoskeleton organization
p.adjust
= 0.0287
0.0
2.5
5.0
7.5
10.0
12.5
Count
C
CLASP2 S327
delta (Post−Pre)
0.00
−0.25
−0.50
−0.75
−1.00
Insulin
Exercise
D
CLASP1 S600
delta (Post−Pre)
0.6
0.4
0.2
0.0
Insulin
Exercise
E
CLASP1 S559
delta (Post−Pre)
0.0
−0.2
−0.4
−0.6
Insulin
Exercise

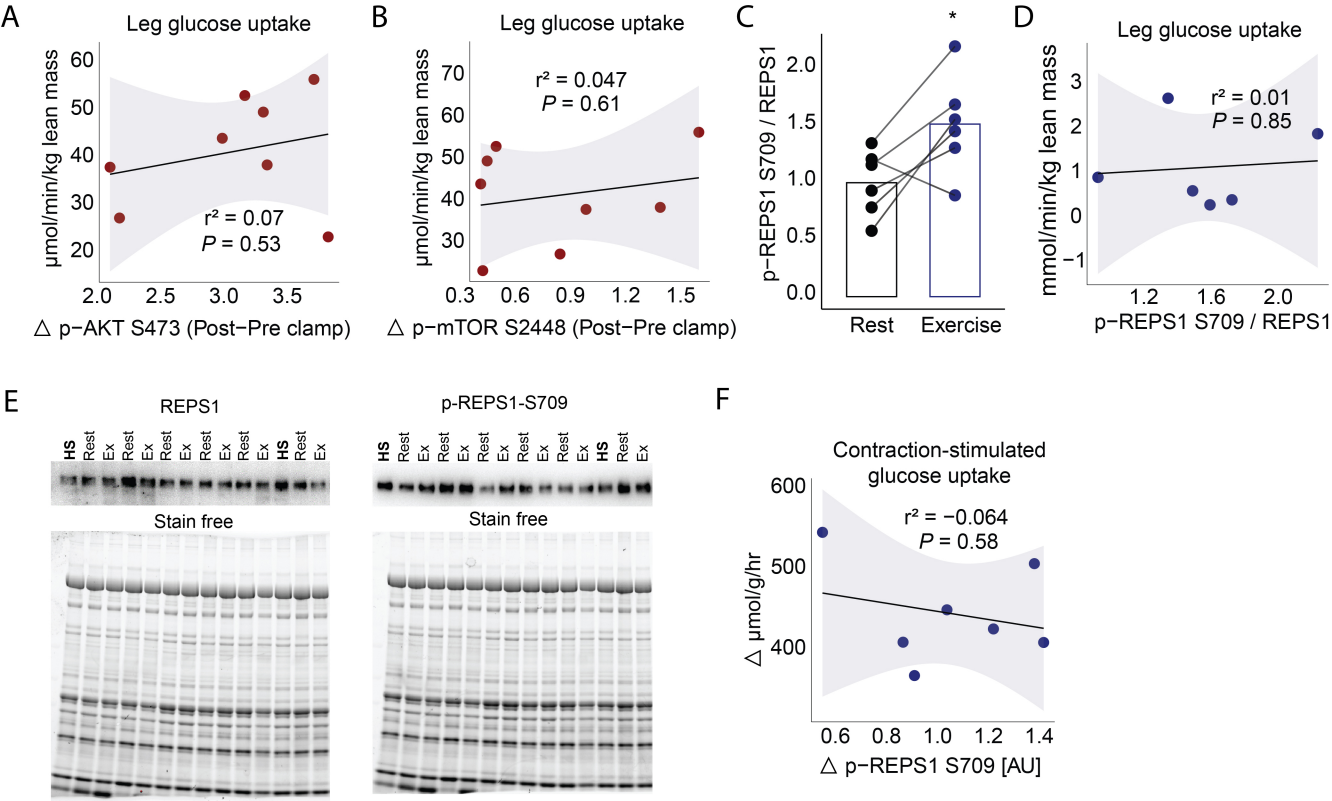
A
Leg glucose uptake
μmol/min/kg lean mass
r² = 0.07
P = 0.53
Δ p−AKT S473 (Post−Pre clamp)
B
Leg glucose uptake
μmol/min/kg lean mass
r² = 0.047
P = 0.61
Δ p−mTOR S2448 (Post−Pre clamp)
C
p−REPS1 S709 / REPS1
Rest
Exercise
D
Leg glucose uptake
mmol/min/kg lean mass
r² = 0.01
P = 0.85
p−REPS1 S709 / REPS1
E
REPS1
p-REPS1-S709
HS Rest Ex Rest Ex Rest Ex Rest Ex Rest Ex HS Rest Ex
Stain free
F
Contraction-stimulated glucose uptake
Δ μmol/g/hr
r² = −0.064
P = 0.58
Δ p−REPS1 S709 [AU]

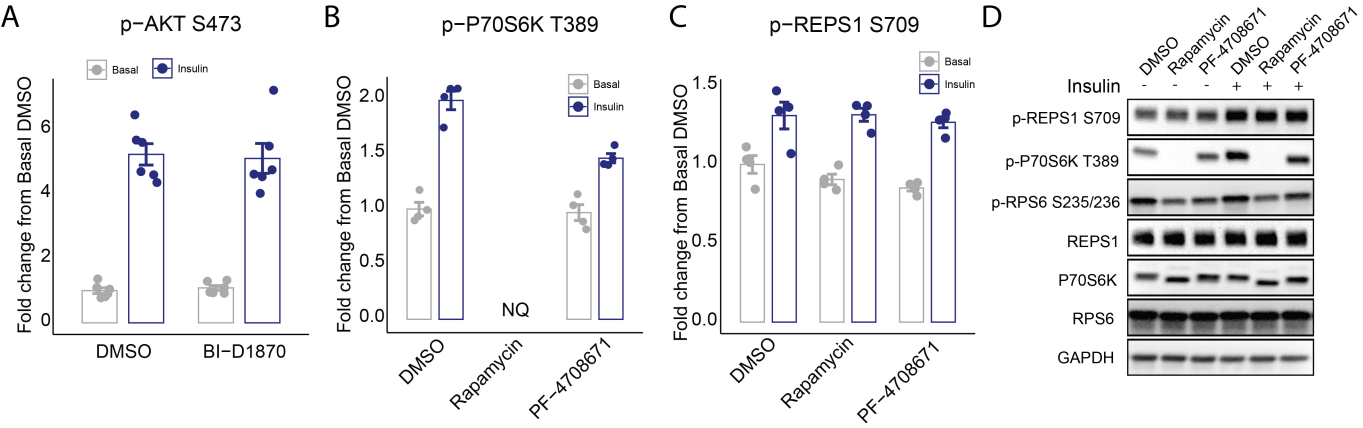

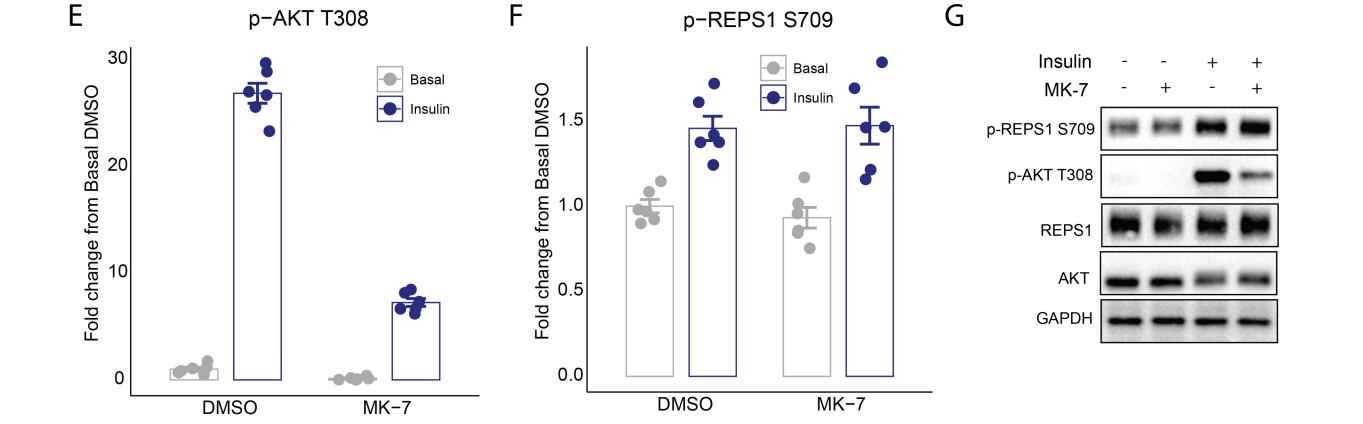

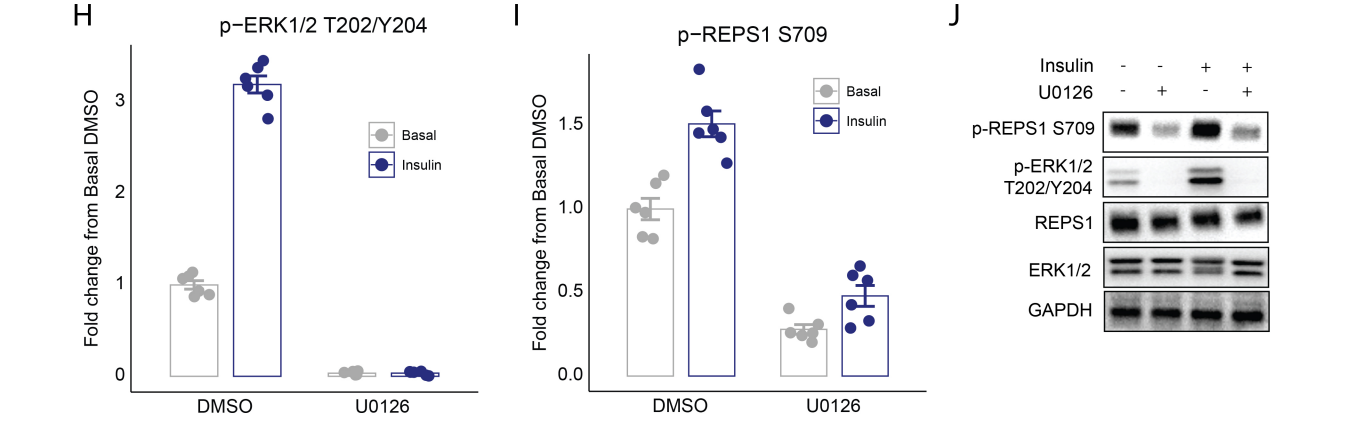

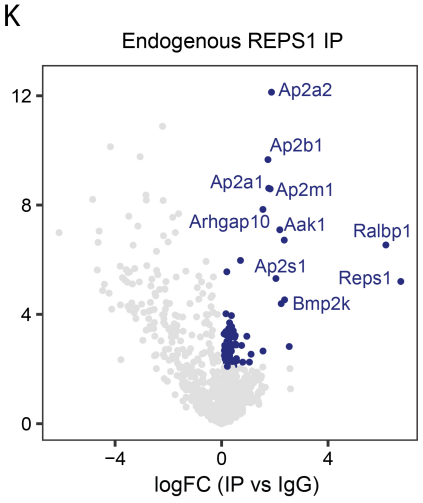

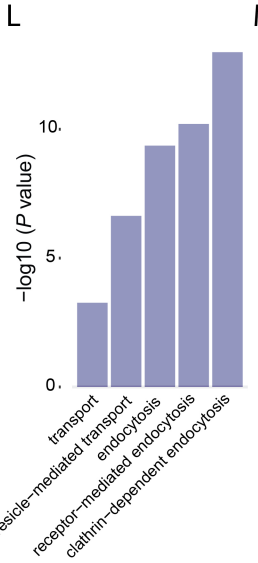

M

logFC(WT-CTR)	logFC(IP-IgG)	Gene name	Protein ID
6,4	7,1	Reps1	O54916
5,9	6,7	Ralbp1	Q62172
5,1	2,4		Q6PIU9
4,7	2,2	Aak1	Q3UHJ0
2,6	2,3	Bmp2k	Q91Z96
2,0	1,8	Ap2a1	P17426
1,9	1,7	Ap2b1	Q9DBG3
1,8	1,7	Arhgap10	Q6Y5D8
1,7	1,8	Ap2m1	P84091
1,7	2,1	Ap2s1	P62743
1,6	1,9	Ap2a2	P17427
1,6	1,3		Q3U6N9
0,5	0,2	Hmga2	P52927
0,2	0,4	Klhl30	Q8C3F7
0,2	0,2	Gipc1	Q9Z0G0
0,2	0,1	Tial1	P70318
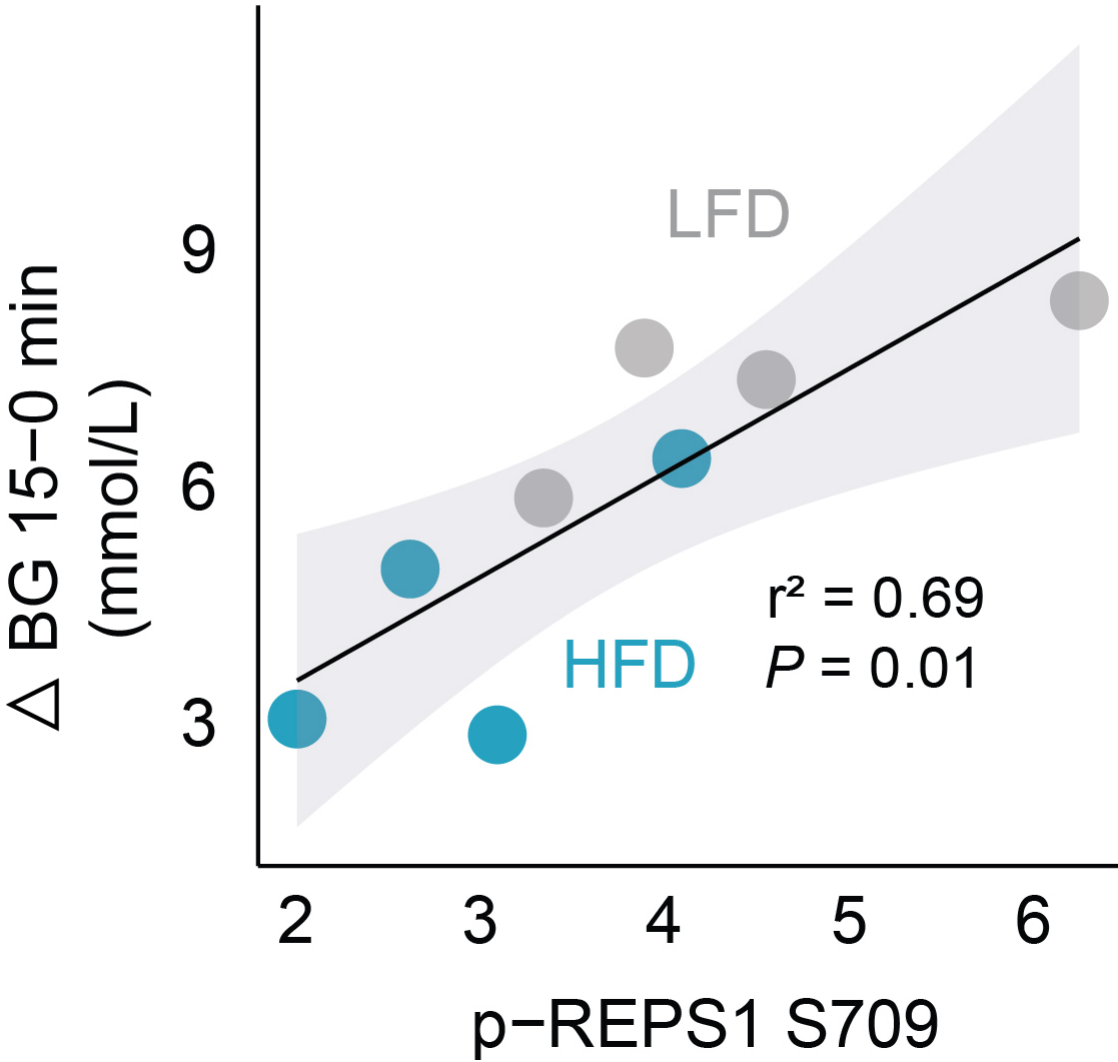
A